Long-term live imaging reveals cytosolic immune responses of host hepatocytes against *Plasmodium* infection and parasite escape mechanisms

Monica Prado[2]*, Nina Eickel[1]*, Mariana De Niz[1], Anna Heitmann[2], Carolina Agop-Nersesian[1], Rahel Wacker[1], Jacqueline Schmuckli-Maurer[1], Reto Caldelari[1], Chris J. Janse[3], Shahid M. Khan[3], Jürgen May[4], Christian G. Meyer[5,6], Volker T. Heussler[1,7]

[1]Institute of Cell Biology, University of Bern, Bern, Switzerland

[2]Molecular Parasitology, Bernhard Nocht Institute for Tropical Medicine, Hamburg, Germany

[3]Center of Infectious Diseases, Leiden University Medical Center, Leiden, The Netherlands

[4]Infectious Disease Epidemiology, Bernhard Nocht Institute for Tropical Medicine, Hamburg, Germany

[5]Molecular Medicine, Bernhard Nocht Institute for Tropical Medicine, Hamburg, Germany

[6]Institute of Tropical Medicine, Eberhard-Karls University, Tübingen, Germany

* These authors contributed equally

[7]Corresponding author: Volker Heussler, Institute of Cell Biology, University of Bern, Baltzerstrasse 4, 3012 Bern, Switzerland

Tel.: + 41 31 631 4650; fax.: + 41 31 631 4615.

E-mail address: heussler@izb.unibe.ch

Keywords: *Plasmodium* liver-stage, malaria, selective autophagy, cytosolic immune response, LC3, ubiquitin, long term live imaging

Abbreviations: PVM, parasitophorous vacuole membrane; STED, stimulated emission depletion; LC3, light chain 3; LAP, LC3-associated phagocytosis; PE, phosphatidylethanolamine; IFA, immunofluorescence assay; GFP, green fluorescent protein; RFP, red fluorescence protein; Pb, *Plasmodium berghei*; WT, wild type; EM, electron microscopy; MEFs, mouse embryonic fibroblasts; ATG, autophagy related; ATG4, autophagy-related 4; ATG7, autophagy-related 7; ATG3, autophagy-related 3; ATG12, autophagy-related 12; ATG5, autophagy-related 5; ATG16, autophagy-related 16; ATG8, autophagy-related 8; *Atg5-/-* , autophagy-related 5 knockout; PV, parasitophorous vacuole; PM, parasite membrane; UIS4, upregulated in infectious sporozoites gene 4; LAMP 1, Lysosomal-associated membrane protein 1; spz, sporozoite; e-schz, early schizont; l-schz, late schizont; CathD, cathepsin D; Exp1, exported protein 1; SQSTM1, sequestosome 1; mTOR, mammalian target of rapamycin; HepG2, human hepatoma cells; ECACC, European Collection of Cell Cultures; MEM, minimum essential medium; FCS, fetal calf serum; DMEM, Dulbecco's modified Eagle Medium; CLS, confocal line scanning; DAPI, 4',6-diamidino-2-phenylindole; DNA, deoxyribonucleic acid; hpi, hours post infection; FACS, fluorescent-activated cell sorting; PBS, phosphate-buffered saline; CSP, circumsporozoite protein; EBSS, Earles's balanced salt solution; aa, aminoacids; PbmC, *Plasmodium berghei* expressing mCherry fluorescent protein; SD, standard deviation

Abstract

Plasmodium **parasites are transmitted by** ***Anopheles*** **mosquitoes to the mammalian host and actively infect hepatocytes after passive transport in the bloodstream to the liver. In their target host hepatocyte, parasites reside within a parasitophorous vacuole (PV). In the present study it was shown that the parasitophorous vacuole membrane (PVM) can be targeted by autophagy marker proteins LC3, ubiquitin, and SQSTM1/p62 as well as by lysosomes in a process resembling selective autophagy. The dynamics of autophagy marker proteins in individual** ***Plasmodium berghei*****-infected hepatocytes were followed by live imaging throughout the entire development of the parasite in the liver. Although the host cell very efficiently recognized the invading parasite in its vacuole, the majority of parasites survived this initial attack. Successful parasite development correlated with the gradual loss of all analyzed autophagy marker proteins and associated lysosomes from the PVM. However, other autophagic events like non-selective canonical autophagy in the host cell continued. This was indicated as LC3, although not labeling the PVM anymore, still localized to autophagosomes in the infected host cell. It appears that growing parasites even benefit from this form of non-selective host cell autophagy as an additional source of nutrients, as in host cells deficient for autophagy, parasite growth was retarded and could partly be rescued by the supply of additional amino acid in the medium. Importantly, mouse infections with** ***P. berghei*** **sporozoites confirmed LC3 dynamics, the positive effect of autophagy activation on parasite growth, and negative effects upon autophagy inhibition.**

Introduction

Plasmodium parasites are the causative agents of malaria, a disease that still affects more than 300-500 million people and kills several hundred thousands yearly. *Plasmodium* parasites are transmitted by *Anopheles* mosquitoes and injected into the skin of the vertebrate host as motile sporozoites. For further development, these sporozoites have to first find their way to a blood vessel[1] before being transported passively by the blood stream to the liver. Within the liver, motile sporozoites migrate along the endothelia and pass through Kupffer cells or endothelial cells to reach their target hepatocyte.[1] Sporozoites transmigrate through a number of hepatocytes, until finally settling in one where they undergo growth and asexual replication. Sporozoites invade their host cell by invagination of the host cell plasma membrane and the formation of a parasitophorous vacuole membrane (PVM). Upon invasion, the parasite massively modulates the PVM by export of numerous proteins. Although it has been speculated that proteins are also secreted into the host cell, and that they can manipulate host cell signaling, so far this observation has been confirmed only for very few proteins.[2] Inside the parasitophorous vacuole (PV), rodent *Plasmodium* species transform within the first 16 hours to a trophozoite, and later, a schizont stage. The liver schizont stage is characterized by an extraordinary growth and nuclear replication that lasts approximately 30 hours. In the last few hours of liver stage development, the parasite plasma membrane starts to invaginate, forming thousands of merozoites that are released into the host cell cytoplasm upon PVM rupture. PVM rupture induces an ordered form of host cell death that is characterized by host nucleus condensation but not by fragmentation of the DNA.[3] Importantly, merozoites accumulate Ca2+ released from host cell stores during cell death and thus block exposure of phosphatidylserine residues to the outer leaflet of the

membrane of the infected cell. Host cell death also allows the formation of merosomes, vesicles that bud from the host cell membrane and are filled with merozoites. By a so far unknown mechanism, merosomes are pushed into the blood vessel while merozoites continue to be transported in the budding vesicle. Merosomes are liberated and transported into the lung capillaries where they release merozoites to initiate infection of red blood cells, marking the beginning of the pathogenic phase of the infection.[4]

In our present work, we studied two main types of autophagy that influence parasite establishment, growth and development: on one hand, the host cell response selectively targeting *Plasmodium* parasites (selective autophagy), and on the other hand non-selective canonical autophagy potentially supporting parasite nourishment. Recently it has been shown that the autophagy marker protein LC3 is recruited to the PVM and to tubules budding from the PVM[5] but nothing is known about canonical host cell autophagy and its effect on parasite development.

Although intracellular pathogens like *Plasmodium* avoid direct contact with the host adaptive or innate immune responses, the invaded host cell is also equipped with a plethora of mechanisms to eliminate the invader.[6,7] These mechanisms can be considered to be cytosolic immune responses. One prominent cytosolic immune mechanism is selective autophagy, which also serves as a catabolic process to recycle damaged organelles or large protein complexes.[8] Selective autophagy differs from canonical autophagy in that it specifically targets intracellular pathogens or intracellular components by ubiquitination, and does not induce the general autophagy response of the cell that is elicited upon starvation. Similar to canonical autophagy, upon selective autophagy, double-membrane structures called phagophores form around invaded pathogens or damaged organelles.

Another autophagy-related response of host cells to pathogens residing in a vacuole is to directly target the vacuolar membrane and label it for fusion with lysosomes in a process called LC3-associated phagocytosis (LAP).[9] LC3 targeting of membranes is a common feature of most autophagy-related processes.[10,11] LC3 is a ubiquitous cytosolic protein and, like other proteins of the autophagy machinery, it is constitutively expressed[8] and can be immediately recruited when autophagy is induced. LC3 is synthesized as a precursor and the C-terminus is processed by the cysteine protease ATG4. This generates LC3-I, in which a C-terminal glycine becomes exposed, thus becoming available for the subsequent conjugation reactions. LC3-I is activated by ATG7, transferred to the E2-like enzyme ATG3, and finally, with the help of the ATG12-ATG5-ATG16 complex (which acts as an E3-like enzyme), conjugated with phosphatidylethanolamine (PE) to form LC3-II. In canonical autophagy, LC3-II localizes to target membranes such as autophagosomal membranes. In non-canonical autophagy processes such as LAP, LC3-II localizes to membranes of pathogen-containing compartments. Due to the different localization patterns of LC3-I and LC3-II, LC3-II is considered to be a key marker protein for all different forms of autophagy.[9-11]

Several pathogens have developed strategies to circumvent autolysosomal degradation.[12-14] It has been shown that *Toxoplasma gondii* interferes with Akt signaling to block autophagy but it has also been suggested for the same parasite that it even can exploit autophagy as an additional source of nutrients.[13] An explanation for these results, which at first glance may seem contradictory, might be the difference of selective autophagy that needs to be controlled by the parasite to avoid elimination, and canonical autophagy that might be exploited by the pathogen.

In the present study, the autophagic response of hepatocytes to the invasion of *Plasmodium* sporozoites was examined. Since biochemical analysis of

Plasmodium-infected hepatocytes is limited by the low infection rate, we developed long-term live imaging to follow individual infected cells. This approach allowed us to record for the first time the entire 64-hour development period of individual parasites that successfully invaded a hepatocyte, developed into merozoites, and were released into the host cell cytoplasm, thereby inducing cell detachment *in vitro*. We found that the invaded *Plasmodium* sporozoites failed to control the initial LC3 labeling of the PVM and some were even eliminated by autophagy. However, the surviving parasite majority appeared to be able to control the progression of the autophagic process by an as-yet unknown mechanism. Indeed, these surviving parasites appeared to benefit from non-selective canonical autophagy as an additional source of nutrients.

Results

The host cell recognizes and labels invading sporozoites

To analyze the selective autophagy-related mechanisms that arise while *Plasmodium* is infecting hepatocytes, we used the murine malaria model *Plasmodium berghei*. We first examined whether sporozoite infection of hepatocytes causes the cytosolic LC3 protein to localize to autophagosomes. Immunofluorescence analysis (IFA) of *P. berghei*-infected primary hepatocytes stained with an anti-LC3 antibody revealed that the localization of endogenous LC3 differed depending on the stage of parasite development (**Fig. 1A**). During sporozoite invasion, LC3 accumulated in membranous structures around the parasite, whereas in late schizogony LC3-positive vesicles were more randomly distributed throughout the cytoplasm of the host cell.

Although the original observation of LC3 accumulation around early parasite stages was made in primary mouse hepatocytes, it was essential to validate this observation *in vivo*. To follow the dynamic events of LC3 recruitment after sporozoite invasion, we

used mCherry-expressing parasites to infect transgenic mice that express in all nucleated cells LC3 N-terminally tagged with green fluorescent protein (GFP). Intravital imaging of the liver of an infected mouse revealed a pattern of LC3 distribution around the parasite in the early developmental stages, which was not seen in the later stages (**Fig. 1B**) that resembled the pattern we also observed *in vitro* (**Fig. 1A**). Importantly, intravital imaging indicated that even late-stage parasites are occasionally eliminated in an autophagy-typical manner (**Fig. 1C; Vid. S1**). This phenomenon was also observed *in vitro* (**Vid. S2**). Since the same effect was observed *in vitro* and *in vivo* it could be concluded that LC3 accumulation around the parasite is indeed a physiological event and not restricted to *in vitro* cultivated cells. It further proves that both, the *in vitro* analysis and the GFP-LC3 mouse are suitable and complementary models for studying autophagy in *Plasmodium*-infected hepatocytes.

To study the dynamics of LC3 localization, we transfected the hepatoma cell line HepG2 with a plasmid encoding GFP-LC3 and infected these cells with *P. berghei* sporozoites expressing the red-fluorescent protein mCherry. Live imaging approaches revealed that in the vast majority of infected cells, GFP-LC3 was immediately and dramatically recruited into a membrane around the parasite after invasion (**Fig. 2A; Vid. S3**). This confirms the IFA data (**Fig. 1A**) and suggests that the host cells recognize the invader and mount a strong cytosolic immune response against it. Thereafter, however, although a considerable number of parasites were indeed eliminated between 9 and 24 hours post-infection (**Fig. 2B**), the LC3 accumulation around the majority of parasites was progressively lost suggesting that the parasites escaped this host cell response (**Fig. 2A; Vid. S4, S5 and S6**).

Before wild-type (WT) LC3 can accumulate around the invaded sporozoite, it must be correctly processed, lipidated, and incorporated into a membrane. When

HepG2 cells were transfected instead with a plasmid encoding the GFP-LC3^{G120A} mutant, which cannot be processed and lipidated[10], mutant LC3^{G120A} was not mobilized around the invaded parasite (**Fig. S1**) suggesting that processing and lipidation are prerequisites for the observed LC3 accumulation around the parasite. It is important to note that the cells transfected with the GFP-LC3^{G120A} mutant construct still express the endogenous and thus functional LC3. Therefore, it is unlikely that expression of the GFP-LC3^{G120A} mutant would affect parasite development.

Next, we wanted to know whether the host cell isolates the parasite in an autophagosome. Electron microscopic (EM) analysis of *P. berghei*–infected HepG2 cells did not reveal the formation of a typical autophagosomal membrane around the invading parasite (**Fig. 2C**) confirming previous EM studies examining in great detail *P. berghei* development *in vitro* and *in vivo*.[15-17] This hinted that upon sporozoite invasion, LC3 must be incorporated into another membrane.

One such membrane may be the PVM, which is a membrane that surrounds parasites. Indeed, when *P. berghei*-infected HepG2 cells were stained with an antiserum against the PVM marker protein UIS4 and an anti-LC3 antibody, super resolution STED microscopy revealed a clear co-localization of both markers (**Fig. 3A)**.

LC3 labeling of the PVM during early parasite development was further confirmed by confocal microscopy of GFP-LC3-expressing HepG2 cells additionally stained with an anti UIS4 antiserum (**Fig. 3B**, upper two panels). However, in the later stages, LC3 accumulation around the PVM diminished; instead, the protein formed LC3-positive aggregates around the PVM and throughout the cytoplasm (**Fig. 3B**, lower panel). It is possible that the parasites actively clear the PVM of this autophagy marker protein, most likely to prevent progression of the destructive events in the PV that could result in parasite elimination. Supporting this view is the

fact is that the parasites whose PVMs continued to bear ample amounts of LC3 in the later stages did not complete liver stage development (**Fig. 3C and D; Vid. S7**). Instead, they often underwent a kind of cell death that has been previously reported.[18] Indeed, the late liver-stage schizonts that continued to have an LC3-positive PVM were significantly smaller than the parasites whose PVM lost LC3 (**Fig. 3D**). Thus, LC3 persistence in the PVM is associated with parasite growth arrest and elimination.

Lysosomes are attracted by early-stage and arrested parasites

Having confirmed that LC3 labeling of the PVM and subsequent autophagy-related events can limit parasite infection to a certain extent, we next investigated the events that occur up- and downstream of the labeling of the PVM in infected cells with LC3. A hallmark of autophagy is the fusion of LC3-positive autophagosomes with lysosomes, which generates lysogenic autolysosomes.[19] One study suggested that lysosomes fuse with the PVM in *P. berghei*-infected hepatocytes.[20] We therefore sought to determine i) the dynamics of lysosome fusion in relation to LC3 recruitment to the PVM in infected cells, ii) whether the pH drops in the PV, and iii) whether the lysosomal protease cathepsin D is recruited to the PV.

To follow the dynamics of lysosomes in infected cells and to quantify the corresponding observations, we used several live and indirect staining methods. LAMP1 is a protein of the lysosomal membrane[21] and can either be tagged by GFP or detected by IFA using antibodies. Other methods that we used for live imaging were to employ a RFP-tagged version of cathepsin D,[22] which is the main lysosomal protease and to stain cells with LysoTracker, which detects lysosomes because of the low pH in these compartments. Finally, to visualize protein degradation in lysosomes, DQ-BSA was used. Unprocessed DQ-BSA is colorless because its fluorogenic group

is quenched. On processing, DQ-BSA emits red fluorescence and thus labels degradation vesicles like lysosomes and autolysosomes.

The main observation from the experiments using these different staining approaches was that while lysosomes accumulated around the early-stage parasites, this association was progressively lost during parasite development (**Fig. 4 Fig. S2-S5**). All lysosome markers, namely, LysoTracker, DQ-BSA, cathepsin D, and LAMP1, appeared to be closely associated with the PVM and LC3 (**Fig. S3-S5)** at early parasite stages and show a more random distribution in the host cell at later developmental stages. Furthermore, in the early parasite stages LAMP1 was found to partially co-localize with UIS4 and thus the PVM (**Fig. S3 Vid. S8**), which strongly suggests that the lysosomes fused with the PVM. However, this LAMP1 incorporation into the PVM was eventually lost, similar to what was observed for LC3.

Another important observation of these staining experiments was that the PV did not become positive for LysoTracker, cathepsin D-RFP, or DQ-BSA (**Fig. 4A, S2 and S4**). This suggests that even though the PV fused with lysosomes, this event did not enhance the degradation properties of the vacuole.

Finally, we investigated the fate of the arrested parasites and compared them to normally developing parasites. At later stages, the arrested parasites remained LAMP1-, LysoTracker-, and LC3-positive, which indicated that these parasites were in the process of being eliminated (**Fig. 5 and 3C**). Elimination of an arrested LC3-positive parasite can be observed in Video S5.

These observations together suggest that while the host cells try to isolate the invading parasites in LC3-positive compartments, they are not able to eliminate the majority of these parasites within these vacuoles by acidification through fusion with lysosomes. Thus, even though lysosomes associate with the PVM at an early

stage, the majority of parasites avoid acidification, protease activation and degradation.

LC3 recruitment to the PVM is the result of a novel form of autophagy

There are several pathways that could potentially trigger the observed LC3 labeling of the PVM in *P. berghei*-infected hepatocytes. One is LAP, which is characterized by a series of clearly defined molecular events.[9,23] A hallmark of LAP is the initial labeling of the target membrane by phosphatidylinositol 3-phosphate (PI(3)P) and a transient labeling by Beclin-1. Since we did not find (PI(3)P) and Beclin-1 in the PVM (data not shown) and because we have identified ubiquitin and SQSTM1 localization to the PVM (see below), we excluded LAP as a possible mechanism.

Another process that targets LC3 to a membrane is selective autophagy, in which target membranes are labeled with ubiquitin and the adaptor protein SQSTM1 that then recruits LC3.[24-27] However, in selective autophagy, a newly formed phagophore is generated to isolate the target compartment.[8] Since the presence of this additional membrane was excluded by EM analysis (**Fig. 2**), selective autophagy as it has been characterized so far was also excluded as a possible autophagic mechanism as well.

To our surprise, we then found that the PVM became positive for ubiquitin, SQSTM1, and LC3, all with very similar kinetics (**Fig. 6A and B, Fig. 7A and B; Vid. S9**). Still, so far it is not clear whether ubiquitination is connected with labeling of the PVM with LC3 and lysosomes. To exclude the possibility that ubiquitination of the PVM depends on LC3, we infected GFP-ubiquitin-expressing *Atg5-/-* and control MEFs with *P. berghei* sporozoites. Although the *Atg5-/-* MEFs are deficient in LC3 processing and lipidation,[28] both cell lines showed early ubiquitination of the PVM

(**Fig. 6C**). This further supports the hypothesis that a mechanism related to selective autophagy is activated on *P. berghei* invasion.

Importantly, in infected HepG2 cells the PVM of arrested parasites stayed positive for all markers, namely, ubiquitin, SQSTM1 (**Fig. 8A and B**), and LC3 (**Fig. 3C**). This suggests that this PVM labeling pattern associates with parasite elimination. However, the majority of parasites escaped this advanced stage of autophagy. The molecular basis of this escape mechanism is currently unknown.

Galectins do not mediate labeling of the PVM

Galectins have been shown to target damaged bacteria-containing vacuoles for autophagy, in order to defend cells against bacterial invasion.[29] To investigate whether galectins are also recruited to the PVM in *P. berghei*-infected cells, we transfected HepG2 cells with constructs that allow expression of fluorescently tagged galectin 1, 3, 8 and 9. When we infected these transfected cells with *P. berghei* sporozoites we did not observe a marked labeling of the PVM, suggesting that none of the galectins investigated play an important role the recruitment of LC3 to the PVM (**Fig. S6A-C**).

Starvation-induced autophagy promotes parasite growth and survival

To test whether enhanced autophagy has an effect on parasite development we wanted to analyze parasite development *in vivo* under starvation conditions. For that we generated a *P. berghei* ANKA reporter line (PbmCherry$_{hsp70}$+Luc$_{eef1\alpha}$), which expresses luciferase under the control of the *eef1α* (PBANKA_113330) promoter and, in addition, mCherry under the control of *hsp70* (PBANKA_071190) promoter (**Fig. S7A-D)**. Parasites of this line express luciferase and mCherry throughout the life

cycle. The life cycle progression of this line in the blood, mosquito and liver stage development is comparable to that of wild type *P. berghei* ANKA parasites (**Fig. S7E).** Balb/c mice were starved and infected with the luciferase-expressing *P. berghei* line PbmCherry$_{hsp70}$+Luc$_{eef1\alpha}$, and parasite growth in the liver was monitored until transition to the blood stage (**Fig. 9A**). We followed two different regimens: mice were either pre-starved 12 hours before infection or they were starved upon infection. Surprisingly, both starvation regimens resulted in an increased parasite load in the liver with a peak at 48 hpi (**Fig. 9B**). To analyze whether starvation induces canonical autophagy, GFP-LC3 mice were starved and monitored by intravital imaging 30 hours later (**Fig. S8**). Significantly higher numbers of GFP-LC3 positive autophagosomes upon starvation indeed confirmed increased autophagy levels. Together, canonical non-selective autophagy appears to even support parasite development in hepatocytes.

To examine whether the increased parasite load is due to more surviving parasites or increased parasite growth, Balb/c and C57B/6 mice were infected with *P. berghei* and the size and the numbers of intracellular parasites were analyzed on histological sections (**Fig. 9C and D**). Liver sections of non-starved mice served as control. At 24 hpi the number of parasites was significantly increased in the starved animals; this was even more pronounced at 36 and 44 hpi. The fact that in starved animals the relative number of parasites was higher at later stages indicates that the number of control parasites must have decreased over time. This confirms our original *in vitro* observations that a considerable number of parasites are eliminated during their development from sporozoite to liver schizont. Importantly, although the absolute number of infected hepatocytes differed substantially among Balb/c and C57B/6 mice, there was no significant difference in the relative number in both mouse strains when comparing starved and control mice. In conclusion starvation-induced

autophagy had similar effects on parasite development independent of the mouse strain used suggesting very general autophagy mechanisms in different mouse stains. This confirms that both animal models are suited to study autophagy-related events upon *Plasmodium* infection.

Drug-mediated manipulation of autophagy has a profound effect on parasite growth and survival

To confirm that inducing canonical autophagy has a positive effect on parasite development, an *in vivo* drug-based approach was employed. Rapamycin is a well-known inhibitor of the gatekeeper of autophagy, mTOR and thus a strong inducer of autophagy. Chloroquine blocks autophagy by preventing the fusion of lysosomes with autophagosomes. Mice were treated with the either of the two drugs, before or after infection with luciferase-expressing *P. berghei* PbmCherry$_{hsp70}$+Luc$_{eef1\alpha}$ sporozoites. As observed in the starvation experiment, the autophagy-inducing drug rapamycin had a strong positive effect on parasite liver load whereas the autophagy inhibitor chloroquine had the opposite effect (**Fig. 10A and B, Fig. S9**). The strongest effects were observed in mice pre-treated with the drugs. In contrast to starvation-induced autophagy, increased parasite load at 40 hpi in rapamycin-treated mice were solely due to increased parasite numbers not to enhanced growth of the parasite in the liver (**Fig. 10C and D**). Interestingly, also chloroquine treatment did not significantly affect parasite size at this time. Lower parasite load in the liver was due to less infected cells at the end of liver stage development. Intravital imaging of GFP-LC3 mice was again employed to confirm that rapamycin induces autophagy (**Fig. S8**). Actually, in comparison to starvation, rapamycin treatment resulted in a dramatically higher number of GFP-LC3 positive autophagosomes.

Together, the *in vivo* experiments strongly suggest that manipulation of autophagy has profound effects on parasite development and growth.

Inhibition of LC3 recruitment to the PVM promotes parasite establishment in host cells

Since starvation and drug treatment can have many off-target effects in mice, we next aimed for a more specific *in vitro* approach to test whether blocking the autophagy machinery affects parasite growth and development. We took advantage of the fact that *P. berghei* sporozoites infect a wide variety of cells, including murine embryonic fibroblasts (MEFs). We used an *Atg5*-/- MEF cell line in which the pathway that leads to LC3 lipidation is blocked.[28] Thus, in *Atg5*-deficient cells, all events that depend on correct LC3 lipidation and membrane association, including autophagy, are interrupted. First, we confirmed that *Atg5-/-* MEFs are deficient in LC3 lipidation upon starvation of the cells by IFA with anti-LC3 antibodies. The knockout and WT MEFs were starved, fixed and stained to analyze LC3 localization (**Fig. 11A**). In WT MEFs, the typical LC3 recruitment to autophagosomes was observed. By contrast, in *Atg5-/-* MEFs, LC3 had a cytoplasmic localization (**Fig. 11A**, left images). Next, we analyzed the dynamics of LC3 in WT and *Atg5-/-* MEFs after infection with mCherry-expressing sporozoites (**Fig. 11A**, right images). While LC3 accumulated in the classical pattern around the parasite in WT MEFS, in infected *Atg5-/-* MEFs it stayed in the cytoplasm. This suggests that the LC3 recruitment observed in WT cells after sporozoite infection is dependent on the typical processing and lipidation of LC3 that is mediated by ATG5.

We next reasoned that if LC3-dependent autophagy is indeed an important mechanism by which the host restricts parasite establishment in its cells, infection of *Atg5-/-* MEFs should result in higher parasite counts. Indeed, the *Atg5-/-* MEF

cultures had more than twice as many infected cells than the WT MEF cultures (**Fig. 11B**). However, the parasites developing in the *Atg5-/-* MEFs were significantly smaller than the parasites that had escaped elimination and continued to reside in the WT MEFs (**Fig. 11C**). This suggests that host cell autophagy may also have beneficial effects for the parasites that manage to escape the first wave of the cytosolic immune response. Since we observed that infected cells not only recruited LC3 to the PVM but also constantly generated typical autophagosomes (**Vid. S10**), we reasoned that successful *Plasmodium* parasites may induce and exploit host cell autophagy to obtain additional amino acids. To test this possibility, we supplemented the medium of sporozoite-infected *Atg5-/-* cells with additional amino acids. Indeed, this rescued the parasite size in these cells (**Fig. 11C**).

Discussion

Host cell response against *Plasmodium* infection. It has become increasingly clear that cells try to fight intracellular pathogens by many means.[12] Committing 'suicide' by inducing apoptosis is one possibility; another one is to isolate the pathogen in a compartment and then specifically eliminate it. The latter mechanism is particularly valuable for the host as the infected cell can then introduce pathogen peptides into the MHC presentation system.[30] Presentation via MHC has the additional advantage that it can help to induce a cell-mediated immune response against the infected cells.

Autophagy is an important and well-studied cytosolic immune response. In selective autophagy, newly formed membranes surround the pathogen that is to be eliminated.[12] These membranes are labeled with LC3-II and later fuse with lysosomes to form degradative autolysosomes. Aside from selective autophagy, recent studies have suggested that there are several other alternative pathways that

have the capacity to eliminate pathogens.[31,32] Most of such pathways are closely related to autophagy and even share the same molecules to execute their tasks. In principle, their main role is to isolate the pathogen in a compartment, to label the membrane of the pathogen-containing compartment, to direct destructive organelles like lysosomes towards these compartments, and finally to fuse these organelles with the membrane of such compartments, thereby releasing their degradative content into the pathogen's hosting niche. Many pathogens, including *Plasmodium* sporozoites, enter the cell by invaginating the host cell membrane and forming a vacuolar membrane. Thus, they are already in an isolated compartment. It has been shown for several invasive bacteria that such already existing compartments can be recognized by the host cell and are labeled by LC3-II.[9,33,34] We have shown here that this also occurs with invading *Plasmodium* sporozoites. Although the entire mechanism for new membrane formation is not needed because the PVM is directly labeled, the pathways that result in LC3 processing and lipidation[35] still appear to be necessary. These pathways include two ubiquitin-like conjugation systems. If one of these conjugations systems is blocked or the C-terminus of LC3 is altered, correct processing and lipidation will no longer be possible. Indeed, when we expressed the GFP-LC3^{G120A} mutant in HepG2 cells and then infected them with mCherry-expressing parasites, we found that the mutant protein did not incorporate into the PVM membrane. Thus, in *Plasmodium* infection of hepatocytes, like in other infections, LC3 must be properly processed and lipidated before it successfully incorporates into the PVM. We were also able to assess the functional significance of this event by using MEFs in which the *Atg5* gene has been deleted.[28] In these *Atg5-/-* MEFs, we never observed incorporation of LC3 into the PVM and parasite elimination was significantly reduced, confirming that the autophagy-related pathway participated directly in parasite control. The fact that more parasites were detected in the

autophagy-deficient MEFs than in the autophagy-competent MEFs clearly supports the notion that the host cell exerts an active autophagy-related process to eliminate viable parasites, rather than the dying parasites simply being removed by autophagy.

While LC3 incorporation into the PVM appears to be an autophagy-related process, it is not a typical selective autophagy since the latter is characterized by the formation of new phagophores. Instead, LC3 incorporation to the PVM resembles LAP more closely. However, LAP is clearly defined by a certain order of molecular events.[36] Since the invasion of bacteria and *Plasmodium* sporozoites are entirely different processes, we expected that the molecular events resulting in LC3 incorporation into the PVM would differ from the events in LAP. Indeed, results from our laboratory strongly suggest that LC3 incorporation into the PVM does not depend on phosphatidylinositol 3-phosphate and Beclin-1 labeling (data not shown), which are hallmarks of LAP.[36]

The exclusion of canonical autophagy and LAP suggests that *P. berghei*-infected hepatocytes must have an alternative pathway by which LC3 is incorporated into a membrane. Similar to selective autophagy, this new pathway appears to be initiated by ubiquitination, and subsequent association with the linker protein SQSTM1. However, unlike selective autophagy, no new membrane is built around the PVM. Instead, ubiquitin, SQSTM1 and LC3-II all appear to be directly incorporated into the PVM. The fact that *Atg5*-deficient MEFs allow ubiquitination but not LC3-II incorporation supports the idea that ubiquitination precedes LC3-II mobilization, perhaps *via* SQSTM1, which is incorporated into the PVM with similar kinetics as ubiquitin and LC3-II.

Parasite escape from the cytosolic immune response of the host cell. Although our data show clearly that host cells can actively eliminate a considerable number of

parasites, more than half of them evade this response. We still do not know why some parasites are eliminated and others develop normally. We hypothesize that there may be a very fine balance between the parasite and the host cell that determines the outcome of the infection. During schizogony, successful parasites appear to actively remove LC3 from the PVM and avoid continued attack by lysosomes. There are several mechanisms by which the parasite could achieve this. First, it could activate a protease that cleaves LC3. One such protease may be the host-cell ATG4. This protease executes exactly this function during canonical autophagy.[37,38] Another option is that the labeled membrane is shed; the time-lapse movies provided in this study indeed suggest this (in particular in long-term videos S2, S3, and S4). However, this observation needs to be further validated experimentally.

Although it is clear that the parasite has developed strategies that allow it to survive within hepatocytes, many aspects remain to be analyzed. It is not known why the PV of successfully developing parasites does not acidify, despite fusion of the PVM with lysosomes, as shown in this and a previous study.[20] One possibility is that the PVM contains outward-directed proton pumps. However, this may not be necessary considering that the PVM contains pores for the easy uptake of nutrients of up to 855 Da,[39] and that proton gradients may not be able to form in such an environment because they need tight membranes without pores. It has also been suggested that the PVM fuses selectively with lysosomes with a mild pH. However, how the PVM can select between lysosomes with low and mild pH is not known. It is also not clear why we did not detect DQ-BSA in the PV of normally developing parasites. If lysosomes fuse with the PVM, it can be assumed that their contents are released into the PV. Indeed, it has been shown that gold particles that are taken up by the endocytic pathway of infected host cells can be delivered *via* lysosomes to the

PV and even to the parasite cytoplasm.[20] However, since we have shown in this study that parasites can be isolated and eliminated within autolysosomes, it remains to be determined whether the parasites containing gold particles are still viable.

A recent study showed that in *Plasmodium yoelii*-infected hepatocytes, the phosphorylation of Akt kinase and mTOR is elevated.[40] The authors speculated that this protects the parasites from host cell autophagy. Moreover, the expression levels of typical autophagy marker proteins like LC3 were not increased.[40] Transcriptome and proteome analysis in earlier reports also failed to detect elevation of autophagy-related transcripts or proteins in *Plasmodium*-infected hepatocytes,[41,42] which strongly suggests that transcription of autophagy genes is at least not enhanced. These observations are not contradictory to the data provided in this study. Autophagy can be induced at different levels. On one hand, selective autophagy can immediately be activated without transcriptional activation because all components are already present in the cell.[27] Induced autophagy, on the other hand, relies on transcriptional activation and the production of new proteins. Our results suggest that the new pathway observed in *Plasmodium*-infected hepatocytes does not depend on transcriptional activation of autophagy genes and is thus compatible with the data of the study on *Plasmodium yoelii*-infected hepatocytes described above.[40] It now remains to be determined how the parasite controls the induced autophagy of the host cell.

Canonical non-selective autophagy supports parasite survival and growth. Another interesting aspect of *Plasmodium* infection of hepatocytes was that the successful parasites appeared to benefit from host-cell autophagy, as it provided them with an additional source of nutrients. During schizont development, many autophagic events were observed in infected cells probably because the fast-growing

parasite uses amino acids from the host cell. As such, amino acid starvation is a strong trigger of canonical non-selective autophagy. In fact our *in vivo* and *in vitro* data strongly suggest that activation of non-selective autophagy heavily supports parasite survival and growth. Starvation-mediated as well as drug-activated autophagy resulted in significantly enhanced parasite liver load whereas block of autophagy reduced parasite liver load. Nevertheless, we believe that the autophagy we observed is restricted to the already existing basal autophagy machinery in agreement with observations provided by earlier studies.[40-42]

In summary, we suggest that hepatocytes counter *Plasmodium* parasite infection *via* a novel cytosolic immune reaction, and that the parasite responds by manipulating and modulating this host cell response. We believe that other intracellular parasites, bacteria and viruses may employ similar mechanisms. How this knowledge can be translated into effective treatment strategies against these different pathogens remains to be explored.

Materials and Methods

Ethics statement. This study was carried out in strict accordance with the guidelines of the German Tierschutzgesetz (Animal Rights Laws). Mice were obtained from Charles River Laboratories and were between 6 and 10 weeks of age. The protocol was approved by the Department of Veterinary Affairs of the Hamburg state authorities (Permit Number: FI 28/06). Blood feeding and intravital imaging was performed under ketavet/rompun anesthesia, and all efforts were made to minimize suffering. For the generation of the PbmCherry$_{hsp70}$+Luc$_{eef1\alpha}$ parasite line Swiss mice (OF1 ico, Construct 242; 6 weeks old; 25–26 g; Charles River) were used. All animal

experiments to generate and characterize this line were performed at the LUMC and approved by the Animal Experiments Committee of the Leiden University Medical Center (DEC 12042). The Dutch Experiments on Animals Act was established under European guidelines (EU directive no. 86/609/EEC regarding the Protection of Animals used for Experimental and Other Scientific Purposes).

Parasites

P. berghei-ANKA lines were used to infect mice and cell cultures. *P. berghei*-mCherry[43] and *P. berghei*-GFP[44] constitutively express fluorescent proteins that localize to the cytosol of the parasite. *P. berghei*-Exp1-mCherry[45] express the PVM marker protein Exp1 fused to mCherry under the liver stage specific promoter (PBANKA_100300) at the parasite PVM.

The PbANKA-*230p* GIMO mother line (GIMO$_{Pb\text{ANKA}}$; line 1596cl1) which contains the positive-negative selection marker (SM) cassette, a fusion gene of h*dhfr* (human dihydrofolate reductase; positive SM) and y*fcu* (yeast cytosine deaminase and uridyl phosphoribosyl transferase; negative SM) under control of the constitutive *eef1a* promoter, stably integrated into the neutral *230p* locus (PBANKA_030600) through double cross-over recombination.[46] GIMO$_{Pb\text{ANKA}}$ is a reference *P. berghei* ANKA line that is used to rapidly introduce transgenes without drug-resistance markers.

Generation and analysis of the reporter line PbmCherry$_{\text{hsp70}}$+Luc$_{\text{eef1α}}$

Construct pL1720 was made for generation of reporter line mCherry$_{hsp70}$+Luc$_{eef1α}$ that expresses mCherry reporter under control of the *hsp70* (PBANKA_071190) 5'- and 3'-regulatory sequences and luciferase under the control of the *ee1fα* (PBANKA_113330) 5'-promoter/regulatory sequences and the *pbdhfr/ts* (PBANKA_071930) 3'-regulatory sequences. This construct was used to target the

$GIMO_{ANKA}$ mother line using the 'gene insertion/marker out' (GIMO transfection) procedure.[46] Construct pL1720 was made as follows: first the selectable marker (SM) cassette from pL1661 (containing both 5'*hsp70* and 3'*hsp70* sequences, *tgdhfr/ts* SM, and *230p* targeting regions) was removed by digesting the plasmid with *Sna*BI (Roche, 10997480001) and *Sbf*I (New England Biolabs; R06425) followed by treatment of the DNA fragment with Klenow (Roche, 11008404001) and re-ligation resulting in a plasmid that contains only the 5'*hsp70*-3'*hsp70* sequences and the *230p* (PBANKA_030600) targeting regions; the mCherry coding sequences (excised from pL0047 which contains the 5'*pbeef1α-mCherry*-3'*pbdhfr* cassette) was then introduced into this plasmid using sites *Bam*HI (Roche, 10220612001) and *Not*I (Roche, 11014706001). Next a luciferase expression cassette (5'pbeef1a-LuclAV-3'pbdhfr) excised from pL1098 using *Kpn*I (Roche 11198939001) and *Afl*II (Roche, 11198939001) was introduced into this vector using the same restriction sites. This final construct, pL1720, therefore contains the 5'*hsp70-mCherry*-3'*hsp70* and 5'pbeef1a-LuclAV-3'pbdhfr expression cassettes and *230p* targeting sequences but no SM. This construct was linearized by digesting with *Sac*II (Roche, 11117807001) before transfection. The linear DNA construct was introduced into $GIMO_{ANKA}$ parasites using standard methods of GIMO-transfection.[46] Transfected parasites were selected in mice by applying negative selection by providing 5-fluorocytosine (5-FC) (Sigma, F7129-5G) in the drinking water of mice.[47] Negative selection results in selection of parasites where the h*dhfr*::y*fcu* SM in the *230p* locus is replaced by the mCherry reporter-cassette. Selected transgenic parasites ($mCherry_{hsp70}$) were cloned by the method of limiting dilution.[48] Correct integration of the constructs into the genome of $mCherry_{hsp70}$ parasites was analysed by diagnostic PCR-analysis on gDNA and Southern analysis of pulsed field gel (PFG) separated chromosomes as described.[49] Growth of blood stages (asexual

multiplication rate) of mCherry$_{hsp70}$ parasites was determined during the cloning period as described[50] Gametocyte production (gametocyte conversion rate) was determined as previously described.[51]

Cell culture and infection of HepG2, MEF cells and primary hepatocytes. Human hepatoma cells (HepG2) were provided by the European Collection of Cell Cultures (ECACC) and were maintained in Minimum Essential Medium (MEM) with Earle's salts supplemented with 10% fetal calf serum (FCS), 100 U penicillin, 100 µg/ml streptomycin and 2 mM L-glutamine (all from PAA Laboratories, E15-024, A15-101, P11-010, M11-004). WT and *Atg*5-/- murine embryonic fibroblasts (MEF, kindly provided by N. Mizushima) were maintained in Dulbecco's Modified Eagle Medium (DMEM) supplemented with 10% FCS, 100 U penicillin, 100 µg/ml streptomycin, 2 mM L-glutamine and 1x non-essential amino acids (NEAA) (all from PAA Laboratories, E15-009, A15-101, P11-010, M11-004, M11-003). For the rescue experiments, MEFs were cultured in MEM supplemented as described above with or without extra amino acids (PAA Laboratories, M11-002). The cells were cultured at 37°C and 5% CO_2 and were split using Accutase (PAA Laboratories, L11-007).

Primary mouse hepatocytes were isolated by using the protocol described by Wenshuo Zhang (http://www.mouselivercells.com) with modifications. Briefly, the liver of a freshly euthanized mouse was perfused *via* the portal vein with Hepes Buffer (137 mM NaCl (Sigma-Aldrich, S9888-1KG) , 2.68 mM KCl (Fluka Chemie AG P9541-1KG), 10 mM Hepes, 0.7 mM Na_2HPO_4,(Fluka Chemie AG, 71633-250G) pH 7.6, 100 U penicillin, 100 µg/ml streptomycin, for 10 minutes followed by collagenase IV (100 U/ml) (Worthington Biochemical Corporation, LS004188) in William's Medium E (Bioconcept, 1-48F01-I) containing 2 mM L-glutamine for 10 minutes. The perfusate was drained out of the body *via* the inferior vena cava, which was cut immediately

after starting perfusion. During both perfusion periods, the inferior vena cava was clamped every two minutes for 10 seconds to inflate the liver. The digested liver was then excised rapidly, the liver capsule was disrupted, and the hepatocytes were released by gently shaking the digested liver into William's Medium E with 2 mM L-glutamine. The cells were washed three times by 50 g centrifugation in William's Medium E with 2 mM L-glutamine for 2 minutes. Viability was checked by using the trypan blue exclusion method. Between 100,000 and 200,000 cells were seeded onto glass bottom dishes (MatTek corporation, P35G-1.5-20-C) in growth medium (William's Medium E, 2 mM L-glutamine, 10% FCS, 100 U penicillin, 100 µg/ml streptomycin). The growth medium was replaced 3 to 5 hours after isolation. The cells were cultured at 37ºC and 5% CO_2.

When required, cells were treated with 10 µg/ml DQ^{TM} Red BSA (DQ-BSA red, Molecular Probes, D12051) overnight or 75 nM LysoTracker Red DND-99 (Molecular Probes, L-7528) for 10 minutes. *P. berghei*-ANKA lines were used to infect mice and cell cultures. *P. berghei* WT does not express any fluorescent protein. *P. berghei*-mCherry and *P. berghei*-GFP are phenotypically not different from WT parasites apart from the fluorescence. Sporozoites were prepared from the salivary glands of infected female *Anopheles stephensi* mosquitoes and were incubated with the host cells for 2-4 hours. To infect MEFs, the cell and sporozoite mixture underwent an additional centrifugation step (500xg for 5 minutes) during the incubation. After washing, the infected cells were incubated in the medium described for each host cell type above, which was supplemented with 2.5 µg/ml Amphotericin B (PAA Laboratories, P11-001).

Plasmids. The plasmid EGFP-LC3 was kindly supplied by Jonathan C. Howard, Cologne, Germany and the LAMP1-GFP construct was a kind gift from John Brumel.

pmRFP-LC3 (plasmid 21075)[52] and GFP-Ubiquitin (plasmid 11928)[53] were obtained from Addgene (Cambridge, MA, USA). The plasmid Cathepsin D-mRFP was kindly provided by François Darchen, Paris, France.[22] All galectin constructs were kindly provided by Felix Randow, Cambridge, UK. To generate the plasmid EGFP-LC3^{G120A}, the G120A mutation was introduced into the *LC3* gene in the plasmid EGFP-LC3 by using the 5'-GGGCTCGAGATGCCGTCCGAGAAGACC-3' and 5'-GGGGTCGACTTACACAGCCATTGCTGTCGCGAATGTCTC-3' primers and the restriction enzymes XhoI (New England Biolabs, R0146S) and SacI (New England Biolabs, R0156S).

Transfection of HepG2 and MEF cells.

1x10^6 cells were pelleted by centrifugation. After resuspension in Nucleofector V solution (Lonza, VVCA-1003) for HepG2 cells or MEF1 solution for MEFs (Lonza, VPD-1004), the cells were transfected with 3 µg of either GFP-LC3 DNA, RFP-LC3 DNA, Cathepsin D-mRFP DNA, or GFP-Ubiquitin DNA by using a Nucleofector transfection device (program T-028 for HepG2 cells and T20 for MEFs) according to the manufacturer's instructions. The cells were then seeded onto glass bottom dishes for live cell imaging or onto 24 well plates on cover slips for IFA analysis.

Indirect immunofluorescence analysis. After the indicated time points, the infected cells were fixed in 4% paraformaldehyde in PBS for 20 minutes at room temperature. Subsequently, they were either incubated in ice-cold methanol for 10 minutes at -20ºC (for the anti-LAMP1 and -UIS4 antibodies) or permeabilized by using 10 µg/ml Digitonin (for the anti-LC3 antibody) (Sigma-Aldrich, D141-100MG) or 1% Triton X-100 (Fluka Chemie, T8787-250ML) in 10% FCS/PBS (for the anti-ubiquitin and anti-SQSTM1 antibodies). After washing with PBS, the non-specific binding sites were

blocked by incubation in 10% FCS/PBS for 1 h at room temperature. The primary antibodies were diluted in 10% FCS/PBS and then added to the culture. After 1 h at room temperature, the cells were washed with PBS. For detection, the cells were incubated with secondary antibodies for 30-60 minutes at ambient temperature. The nuclei were stained with 1 µg/ml DAPI (Invitrogen, D-1306). The cells were washed again with PBS and mounted on microscope slides with Dako Fluorescent Mounting Medium (Dako, S3023). For live imaging, the nuclei were stained with Hoechst 33342 (Sigma-Aldrich, B2261).

The primary antibodies that were used were mouse monoclonal anti-GFP (BD Biosciences, 565197), rat monoclonal anti-RFP (Chromotek, 5f8), mouse monoclonal anti-LC3 (MBL international, M152-3), rabbit polyclonal anti-UIS4 (kindly provided by P. Sinnis), chicken polyclonal anti-EXP1 (Heussler Lab, BNITM, Hamburg, Germany), mouse monoclonal anti-ubiquitin (Enzo life science, BML-PW8810, clone FK2), rabbit monoclonal anti-SQSTM1/SQSTM1 (MBL international, PM045), and mouse monoclonal anti-hLAMP1 (Developmental Studies Hybridoma Bank, H4A3). Secondary antibodies were anti-rabbit Alexa Fluor® 594 (Invitrogen, A21207), goat anti-rabbit Alexa Fluor® 488 (Invitrogen, A11034), anti-mouse Alexa Fluor® 488 (Life technologies, A21202), anti-mouse Alexa Fluor® 594 (Invitrogen, A11032), anti-rat Alexa Fluor® 594 (Invitrogen, A11007), anti-rat Alexa Fluor® 488 (Invitrogen, A21208), and anti-chicken Alexa Fluor® 594 (Invitrogen, A11042).

Live cell imaging and time lapse microscopy. Confocal laser line scanning (CLS) was performed with a Zeiss Observer Z1 inverted microscope integrated into a laser-scanning microscope (LSM5). Images were acquired by using a Zeiss 63 x Plan-Apochromat 1.4 oil objective and the Zeiss Efficient Navigation 2008 and 2009

software. During imaging, the cells were maintained in a CO_2 (5%) incubator at 37ºC. Images of fixed cells were generated by a confocal laser point scanning microscope (Olympus FV1000 confocal microscope) or by using the Leica DM12000B widefield epifluorescence microscope (Wetzlar, Germany). Contrast and brightness levels were optimized by using either the Zeiss Efficient Navigation 2009 (Jena, Germany), the ImageJ (NIH, USA) software, or Adobe Photoshop. Images were processed as a whole.

To monitor parasite development, the size of parasites was determined by using the density slice module of the OpenLab software version 5.0.2 or ImageJ.

Intravital microscopy was performed as previously described[54] by using the LSM 510 Zeiss microscope in the LSM 5 live mode. Images were acquired by CLS microscopy using a Zeiss Plan Apochromat 63x/1.40 oil DIC M27 objective and the Zeiss LSM 5 Duo Release Version 4.2. GFP-LC3 mice (kindly provided by K. Mizushima[11]) were infected with mCherry-expressing parasites and intravital imaging of an infected liver lobe of an anesthetized mouse was performed at the indicated time points. Image processing was performed by using ImageJ.

Super Resolution Microscopy. For dual-color stimulated emission depletion (STED) microscopy, hepatocytes infected with *P. berghei* sporozoites were fixed 24 h.p.i. with 4% (w/v) paraformaldehyde in PBS followed by 15 min permeabilization in 0.1% Triton-X and 1 h incubation in 10% FCS/PBS blocking buffer. Cells were stained over night by 4°C with 10 µg/ml of anti-LC3 (MBL international, M152-3) and anti-UIS4 (kindly provided by Photini Sinnis) and labeled with 2 µg/ml Oregon Green-488 goat anti-mouse IgG (H+L) (Molecular Probes, Invitrogen, O-6380) and Abberior STAR 440SX goat anti-rabbit IgG (Abberior GmbH, 2-0012-003-4) at room temperature for 1 h. Samples were embedded in Mowiol® 4-88 (Roth, 0713.1)

containing 2.5% DABCO® (Roth, 0718.1) antifade.

Microscopy was conducted on the Leica TCS SP8 inverted microscope equipped with gated STED system and a HC PL APO STED WHITE 100x/1.4 oil immersion objective (Leica Microsystems, Wetzlar, Germany). Depletion was performed with a 592 nm depletion laser and images acquired with a time delay of T *g* = 0.5 ns. Z-Stacks were obtained with increments of 0.22 µm and subsequently deconvolved with the Huygens STED Deconvolution software (Scientific Volume Imaging, Hilversum, Netherlands) and further processed with the image analysis software FIJI[55].

Electron microscopy. Infected HepG2 cells were FACS-sorted to enrich for infected cells and seeded on Thermanox coverslips. At 48 hours post-infection, the cells were washed twice with PBS, fixed with 2% glutaraldehyde (Electron Microscopy Sciences, 16210) in sodium-cacodylate buffer, pH 7.2 and postfixed with 1% osmium tetroxide (Sigma-Aldrich, 201030-1G). The samples were then dehydrated by using a series of increasing ethanol concentrations and propylene oxide. The cells were embedded in an epoxy resin (Epon). Ultrathin sections were made by using Ultra Cut E (Reichert/Leica) and stained with uranyl acetate and lead citrate. The sections were then examined with a Tecnai Spirit (Fei) at an acceleration voltage of 80 kV.

Quantification of viable *P. berghei* parasites. HepG2 cells seeded in 96-well µClear® plates (Greiner-Bio-one, 655097) were infected with *P. berghei* expressing mCherry. Two hours post-infection, excess parasites were washed away twice with medium. Rabbit polyclonal anti-CSP antibody (diluted 1:1000) was added to the medium and incubated for 1 h to eliminate extracellular parasites. Cells were washed and the plate was imaged with an IN Cell Analyzer 2000 automated cell imaging

system (GE Healthcare Life sciences, Glattbrugg, Switzerland) (10× objective, 9 fields/well) at 3.5, 9, 24, 33 and 48 h post-infection. The mCherry signal was detected using excitation and emission filters for TexasRed (emission: 579 nm; excitation: 605 nm). The exposure time was 15–30 ms (30 ms for the 3.5 h and 9 h time points and 15 ms for the later time points). IN Cell Developer Toolbox 1.7 was used to analyze the acquired images. Intensity segmentation was used to identify *P. berghei* mCherry. A post-segmentation process (Sieve) was used to exclude 10 μm^2 objects (3.5–24 h) and 20 μm^2 objects (33–48 h). The output was the number of parasites per well in the 9 fields. The results of quadruplicate experiments are displayed graphically (the number of parasites per well at 3.5 h was set at 100%).

Quantification of autophagy and degradation markers. HepG2 cells were infected with *P. berghei* sporozoites and labeled with antibodies specific for different degradation markers, LysoTracker, or DQ-BSA before being monitored by microscopy. Quantification was performed visually by counting the parasites that were stained strongly or weakly by the dye or antibody. For LysoTracker red-, and DQ-BSA red-stained HepG2 cells, and HepG2 cells transfected with cathepsin D-RFP, a strong association was deemed to be the presence of 10 or more positive vesicles in the immediate proximity of the parasite. Fewer than 10 vesicles around the parasite was defined as a weak association. In infected HepG2 cells that were transfected with ubiquitin-GFP or LC3 or stained with anti-SQSTM1 antibody or anti-LAMP-1 antibody, if the signal covered more than 30% of the proximity of the parasite, the association was considered to be strong. If less than 30% of the parasite was covered with these signals, it was deemed to be a weak association. Arrested parasites were those parasites with clear growth impairment, as indicated by their small size.

Preparation of *P. berghei* parasites and mice for bioluminescence imaging

For bioluminescence imaging of liver stage development, $1x10^5$ *P. berghei* sporozoites were collected from salivary glands of infected *Anopheles stephensi* mosquitoes and injected intravenously into female Balb/c mice 8-10 weeks of age. For starvation assays, mice were separated into a group feeding *ad libidum*, a 30h starvation group after infection, and a group starved for 12h prior to infection followed by 18h post-infection. For autophagy inhibition and induction assays, mice were separated into an untreated control group, a group treated with 50mg/kg chloroquine (Sigma-Aldrich, C6628) at 12, 24 and 36hpi; a group treated with 2.5mg/kg of rapamycin (Enzo Life Sciences, BML-A275-0005) at 12, 24, and 36hpi; a pre-treated group, treated with 50mg/kg chloroquine 2h prior to sporozoite injection, and then 12, 24 and 36hpi; and a pre-treated group, treated with 2.5mg/kg rapamycin 12h prior to sporozoite injection followed by consecutive treatments at 12, 24 and 36hpi.

Chloroquine was diluted in 0.9% NaCl to a final concentration of 20mg/ml. Rapamycin was dissolved in 100% ethanol to a final concentration of 10mg/ml. For luminescence assays, rapamycin was dissolved in a solution medium consisting of 5% PEG-400 (Sigma-Aldrich, 81170), 5% Tween 80 (Sigma-Aldrich, P4780-500ML), and 4% ethanol (Merk Millipore, 100983). Dilutions of both drugs were prepared at the time of administration. Separate control mice were injected with solution media to exclude the potential of artificial effects in luminescence observations.

Real time *in vivo* bioluminescence imaging of liver stage development

Luciferase activity in all mouse groups was determined by full body imaging of mice using an IVIS Lumina II imager (Caliper Life Sciences, USA). Infected mice under the various fasting and treatment conditions were anaesthetized using the isofluorane

anaesthesia system (XGI-8, Xenogen, Caliper Life Sciences, USA). Measurements were performed at various time points post-infection including 12, 24, 36, 44, 56 and 60h, and days 3 and/or 6 post-sporozoite injection. For firefly luciferase quantitation, anaesthetized mice were injected with 100ul of RediJect D-Luciferin (30mg/ml; Perkin Elmer, 760504) intraperitoneally. Measurements were performed 7-10 minutes after injection of the substrate. Imaging was acquired with a 10cm FOV, medium binning factor, and exposure time of 3 minutes. Quantitative analysis was performed using the Living Image 4.1 software.

Staining and histology of liver tissue sections

Histology sections were generated for measurement of size and numbers of parasites at 40h post-infection in the following sets of mice: control, fasting for 24hpi, fasting for 36h post infection, pre-fasting for 12h and 24h post infection, Rapamycin-treated, and chloroquine-treated. 3 Balb/c and 3 C57B/6 mice were used per condition, and infected with varying doses of sporozoites, ranging from $5x10^4$ to $2x10^5$. At 40hpi, mice were euthanized, perfused with 5ml of 4% PFA in PBS, and livers removed. Both complete livers lobes were further stored in 2% PFA in PBS for a further 12h, and then paraffin-embedded. 10 x 50μm sections of both lobes of each animal from various tissue depths were obtained, and stained with hematoxylin and eosin (H&E). Sections were thoroughly analyzed using a Leica DM 5500 B Upright widefield epifluorescence microsope using a 40x objective for general imaging, and a 100x1.6 oil objective for detailed analysis. Images were obtained using the Leica LAS AF Software, and size measurements performed in ImageJ/Fiji.

Statistical analysis. Two groups were compared by using a two-tailed, unpaired

Student's t-test. All statistical analyses were performed by using Prism version 4.0a for Macintosh, GraphPad Software, San Diego, California, USA. *p* values less than 0.05 were considered to indicate statistical significance.

Acknowledgements

Jonathan Howard, François Darchen and Felix Randow are acknowledged for providing plasmid EGFP-LC3, Cathepsin D-mRFP and all galectin constructs, respectively. The LAMP1-GFP construct was a kind gift from John Brumel. Anti-UIS4 antiserum was kindly provided by Photini Sinnis. Stefanie Graewe is thanked for providing the video S10 and Janic Teutsch for video S6.

We thank the German Academic Exchange Service (DAAD) for supporting MP, the Swiss National Foundation for supporting VH (grant 310030_140691/1), the Indo-Swiss consortium and the EviMalaR EU consortium for financial support. The Microscopy Imaging Centre (MIC) in Bern is thanked for technical support.

REFERENCES

1. Amino R, Thiberge S, Martin B, Celli S, Shorte S, Frischknecht F, et al. Quantitative imaging of Plasmodium transmission from mosquito to mammal. Nature medicine 2006; 12:220-4.
2. Ingmundson A, Alano P, Matuschewski K, Silvestrini F. Feeling at home from arrival to departure: protein export and host cell remodelling during Plasmodium liver stage and gametocyte maturation. Cellular microbiology 2014; 16:324-33.
3. Sturm A, Amino R, van de Sand C, Regen T, Retzlaff S, Rennenberg A, et al. Manipulation of host hepatocytes by the malaria parasite for delivery into liver sinusoids. . Science 2006; 313: 1287-90.
4. Baer K, Klotz C, Kappe SH, Schnieder T, Frevert U. Release of hepatic Plasmodium yoelii merozoites into the pulmonary microvasculature. PLoS pathogens 2007; 3:e171.
5. Grutzke J, Rindte K, Goosmann C, Silvie O, Rauch C, Heuer D, et al. The spatiotemporal dynamics and membranous features of the Plasmodium liver stage tubovesicular network. Traffic 2014; 15:362-82.
6. Jo EK, Yuk JM, Shin DM, Sasakawa C. Roles of autophagy in elimination of intracellular bacterial pathogens. Frontiers in immunology 2013; 4:97.
7. Yano T, Kurata S. Intracellular recognition of pathogens and autophagy as an innate immune host defence. Journal of biochemistry 2011; 150:143-9.
8. Levine B, Mizushima N, Virgin HW. Autophagy in immunity and inflammation. Nature 2011; 469:323-35.
9. Cemma M, Brumell JH. Interactions of pathogenic bacteria with autophagy systems. Current biology : CB 2012; 22:R540-5.
10. Kabeya Y, Mizushima N, Ueno T, Yamamoto A, Kirisako T, Noda T, et al. LC3, a mammalian homologue of yeast Apg8p, is localized in autophagosome membranes after processing. The EMBO journal 2000; 19:5720-8.
11. Mizushima N, Yamamoto A, Matsui M, Yoshimori T, Ohsumi Y. In vivo analysis of autophagy in response to nutrient starvation using transgenic mice expressing a fluorescent autophagosome marker. Molecular biology of the cell 2004; 15:1101-11.
12. Deretic V, Levine B. Autophagy, immunity and microbial adaptations. . Cell host & microbe 2009; 5:527-49.
13. Wang Y, Weiss L, Orlofsky A. Host cell autophagy is induced by Toxoplasma gondii and contributes to parasite growth. . J Biol Chem 2009; 284:1694-701.
14. Muniz-Feliciano L, Van Grol J, Portillo JA, Liew L, Liu B, Carlin CR, et al. Toxoplasma gondii-induced activation of EGFR prevents autophagy protein-mediated killing of the parasite. PLoS pathogens 2013; 9:e1003809.
15. Meis JF, Verhave JP, Jap PH, Hess F, Meuwissen JH. An ultrastructural study of developing stages of exo-erythrocytic Plasmodium berghei in rat hepatocytes. Parasitology 1981; 82:195-204.
16. Meis JF, Verhave JP, Jap PH, Meuwissen JH. Transformation of sporozoites of Plasmodium berghei into exoerythrocytic forms in the liver of its mammalian host. Cell Tissue Res 1985; 241:353-60.
17. Meis JF, Verhave JP, Jap PH, Meuwissen JH. Fine structure of exoerythrocytic merozoite formation of Plasmodium berghei in rat liver. J Protozool 1985; 32:694-9.
18. Eickel N, Kaiser G, Prado M, Burda P, Roelli M, Stanway R, et al. Features of autophagic cell death in Plasmodium liver-stage parasites. Autophagy 2013; 9:568 - 80.
19. Mizushima N, Levine B, Cuervo AM, Klionsky DJ. Autophagy fights disease through cellular self-digestion. Nature 2008; 451:1069-75.
20. Lopes da Silva M, Thieleke-Matos C, Cabrita-Santos L, Ramalho JS, Wavre-Shapton ST, Futter CE, et al. The Host Endocytic Pathway is Essential for Plasmodium berghei Late Liver Stage Development. Traffic 2012; 13:1351–63.

21. Obermuller S, Kiecke C, von Figura K, Honing S. The tyrosine motifs of Lamp 1 and LAP determine their direct and indirect targetting to lysosomes. Journal of cell science 2002; 115:185-94.
22. Yuseff MI, Reversat A, Lankar D, Diaz J, Fanget I, Pierobon P, et al. Polarized secretion of lysosomes at the B cell synapse couples antigen extraction to processing and presentation. Immunity 2011; 35:361-74.
23. Florey O, Overholtzer M. Autophagy proteins in macroendocytic engulfment. Trends in cell biology 2012; 22:374-80.
24. Huang J, Brumell JH. Bacteria-autophagy interplay: a battle for survival. Nature reviews Microbiology 2014; 12:101-14.
25. Jiang X, Chen ZJ. The role of ubiquitylation in immune defence and pathogen evasion. Nature reviews Immunology 2012; 12:35-48.
26. Johansen T, Lamark T. Selective autophagy mediated by autophagic adapter proteins. Autophagy 2011; 7:279-96.
27. Kraft C, Peter M, Hofmann K. Selective autophagy: ubiquitin-mediated recognition and beyond. Nature cell biology 2010; 12:836-41.
28. Kuma A, Hatano M, Matsui M, Yamamoto A, Nakaya H, Yoshimori T, et al. The role of autophagy during the early neonatal starvation period. Nature 2004; 432:1032-6.
29. Thurston TL, Wandel MP, von Muhlinen N, Foeglein A, Randow F. Galectin 8 targets damaged vesicles for autophagy to defend cells against bacterial invasion. Nature 2012; 482:414-8.
30. Puleston DJ, Simon AK. Autophagy in the immune system. Immunology 2014; 141:1-8.
31. Boya P, Reggiori F, Codogno P. Emerging regulation and functions of autophagy. Nature cell biology 2013; 15:713-20.
32. Mehta P, Henault J, Kolbeck R, Sanjuan MA. Noncanonical autophagy: one small step for LC3, one giant leap for immunity. Current opinion in immunology 2014; 26:69-75.
33. Birmingham CL, Brumell JH. Autophagy recognizes intracellular Salmonella enterica serovar Typhimurium in damaged vacuoles. Autophagy 2006; 2:156-8.
34. Dupont N, Lacas-Gervais S, Bertout J, Paz I, Freche B, Van Nhieu GT, et al. Shigella phagocytic vacuolar membrane remnants participate in the cellular response to pathogen invasion and are regulated by autophagy. Cell host & microbe 2009; 6:137-49.
35. Fleming A, Noda T, Yoshimori T, Rubinsztein DC. Chemical modulators of autophagy as biological probes and potential therapeutics. Nature chemical biology 2011; 7:9-17.
36. Lai SC, & Devenish, R. J. LC3-associated phagocytosis (LAP): connections with host autophagy. Cells 2012 1:396-408.
37. Nakatogawa H, Ishii J, Asai E, Ohsumi Y. Atg4 recycles inappropriately lipidated Atg8 to promote autophagosome biogenesis. Autophagy 2012 8:177-86.
38. Geng JaK, D. J. The Atg8 and Atg12 ubiquitin-like conjugation systems in macroautophagy EMBO reports 2008 9 859–64.
39. Bano N, Romano JD, Jayabalasingham B, Coppens I. Cellular interactions of Plasmodium liver stage with its host mammalian cell. International journal for parasitology 2007; 37:1329-41.
40. Kaushansky A, Ye A, Austin L, Mikolajczak S, Vaughan A, Camargo N, et al. Suppression of Host p53 Is Critical for Plasmodium Liver-Stage Infection. Cell reports 2013; 3:630–7.
41. Tarun A, Peng X, Dumpit R, Ogata Y, Silva-Rivera H, Camargo N, et al. A combined transcriptome and proteome survey of malaria parasite liver stages. PNAS 2008; 105 305-
42. Albuquerque S, Carret C, Grosso A, Tarun A, Peng X, Kappe S, et al. Host cell transcriptional profiling during malaria liver stage infection reveals a coordinated and sequential set of biological events. BMC Genomics 2009; 10:270.
43. Graewe S, Retzlaff S, Struck N, Janse CJ, Heussler VT. Going live: a comparative analysis of the suitability of the RFP derivatives RedStar, mCherry and tdTomato for intravital and in vitro live imaging of Plasmodium parasites. Biotechnology journal 2009; 4:895-902.

44. Franke-Fayard B, Trueman H, Ramesar J, Mendoza J, van der Keur M, van der Linden R, et al. A Plasmodium berghei reference line that constitutively expresses GFP at a high level throughout the complete life cycle. Mol Biochem Parasitol 2004; 137:23-33.
45. Graewe S, Rankin KE, Lehmann C, Deschermeier C, Hecht L, Froehlke U, et al. Hostile takeover by Plasmodium: reorganization of parasite and host cell membranes during liver stage egress. PLoS pathogens 2011; 7:e1002224.
46. Lin JW, Annoura T, Sajid M, Chevalley-Maurel S, Ramesar J, Klop O, et al. A novel 'gene insertion/marker out' (GIMO) method for transgene expression and gene complementation in rodent malaria parasites. PloS one 2011; 6:e29289.
47. Orr RY, Philip N, Waters AP. Improved negative selection protocol for Plasmodium berghei in the rodent malarial model. Malaria journal 2012; 11:103.
48. Menard R, Janse C. Gene targeting in malaria parasites. Methods 1997; 13:148-57.
49. Janse CJ, Ramesar J, Waters AP. High-efficiency transfection and drug selection of genetically transformed blood stages of the rodent malaria parasite Plasmodium berghei. Nature protocols 2006; 1:346-56.
50. Annoura T, van Schaijk BC, Ploemen IH, Sajid M, Lin JW, Vos MW, et al. Two Plasmodium 6-Cys family-related proteins have distinct and critical roles in liver-stage development. FASEB journal: official publication of the Federation of American Societies for Experimental Biology 2014; 28:2158-70.
51. van Dijk MR, van Schaijk BC, Khan SM, van Dooren MW, Ramesar J, Kaczanowski S, et al. Three members of the 6-cys protein family of Plasmodium play a role in gamete fertility. PLoS pathogens 2010; 6:e1000853.
52. Kimura S, Noda T, Yoshimori T. Dissection of the Autophagosome Maturation Process by a Novel Reporter Protein, Tandem Fluorescent-Tagged LC3. Autophagy 2007; 3:452-60.
53. Dantuma NP, Groothuis TA, Salomons FA, Neefjes J. A dynamic ubiquitin equilibrium couples proteasomal activity to chromatin remodeling. The Journal of cell biology 2006; 173:19-26.
54. Thiberge S, Blazquez S, Baldacci P, Renaud O, Shorte S, Menard R, et al. In vivo imaging of malaria parasites in the murine liver. Nature protocols 2007; 2:1811-8.
55. Schindelin J, Arganda-Carreras I, Frise E, Kaynig V, Longair M, Pietzsch T, et al. Fiji: an open-source platform for biological-image analysis. Nature methods 2012; 9:676-82.

Figure legends

Figure 1. LC3-II is recruited to the vicinity of *Plasmodium* parasites in primary mouse hepatocytes. **(A)** Primary mouse hepatocytes were freshly isolated, seeded on coverslips, and infected with *P. berghei* that expressed mCherry fluorescent protein (PbmCherry). The infected cells were fixed at different developmental stages

and stained with an anti-LC3 antibody and the DNA dye DAPI. Labeled scale bars are included at the bottom-right of the images. **(B)** *In vivo* LC3 dynamics in *Plasmodium berghei*-infected cells. A GFP-LC3-expressing mouse (green) was infected with mCherry-expressing *P. berghei* parasites (red) and analyzed by intravital imaging at different developmental stages, as indicated. **(C)** Intravital imaging of the same mouse that shows a dying parasite at the late developmental stage. The dispersed parasite vesicles show a transient but strong association with GFP-LC3. Scale bars: 10 μm. See also video S1.

Figure 2. *In vitro* LC3 dynamics in *Plasmodium berghei*-infected cells. (A) HepG2 cells were transfected with a plasmid encoding GFP-LC3, infected with *P. berghei* sporozoites expressing mCherry protein, and monitored at different phases of development. Spz: invaded sporozoites at 4 hours post-infection; e-schz: early schizont at 24 hours post-infection; l-schz: late schizont at 48 hours post-infection; cyt: cytomere stage at 56 hours post-infection. Representative images are shown below the graph. The infected host cells harboring LC3-associated parasites, vesicular LC3, or cytoplasmic LC3 were counted and expressed as percentages. Scale bars: 10 μm. **(B)** To study the dynamics of parasite elimination during liver-stage infection, HepG2 cells were seeded in 96-well plates and infected with mCherry-expressing parasites. To eliminate the extracellular parasites, the infected cells were treated with an anti-CSP antiserum. The parasites were then counted by using an IN Cell analyzer at the indicated time points. The average number of invaded parasites at the sporozoite stage (*i.e.* 3.5 hours post-infection) was considered to be 100%. **(C)** Electron microscopic analysis of *P. berghei*-infected cells during sporozoite transformation and early schizogony. The overview and the

magnifications clearly demonstrate that apart from the parasite membrane (PM) and the parasitophorous vacuole membrane (PVM), no other surrounding membranes are visible. The insets are magnifications of the areas of interest, including PM and PVM. Scale bars of the left image: 200 nm, inset: 100 nm. Scale bars of the right image: 2 µm, inset 100 nm.

Figure 3. Host cell LC3 incorporation into the parasitophorous vacuole membrane (PVM). (A) LC3-RFP-expressing hepatocytes infected with a 24 h liver schizont co-stained with anti-LC3 (green) and the PVM marker UIS4 (red). STED microscopy was perfomed and z-Stacks were obtained with increments of 0.22 µm and subsequently deconvolved. 3D-projection of the PVM shows a direct incorporation of the host cell autophagy marker LC3-II. Quantification of the colocalisation applying the Pearson's coefficient revealed a correlation value of □ = 0.71. The inset shows a magnification of the PVM with strong LC3 incorporation. Scale bar: 2 µm **(B)** GFP-LC3-transfected HepG2 cells were infected with *Plasmodium berghei* sporozoites, fixed at different time points after infection, and stained with antiserum against the PVM marker protein UIS4 (red). To detect GFP-LC3 localization, the cells were also stained with an anti-GFP antibody (green). For the merged picture, the DNA stain with DAPI (blue) was included. Scale bars: 10 µm. (**C)** LC3 persistence in the PVM during schizogony associates with impaired parasite growth. The immunofluorescence analysis images show neighboring infected cells harboring schizonts, one of which is GFP-LC3-positive and small (S). The second is GFP-LC3-negative and larger (L). Staining was performed as described in B. Scale bars: 10 µm. (**D)** The sizes of the LC3-positive and -negative parasites 48 hours post-infection (late schizogony) were measured and compared statistically. p <0.0001.

Figure 4. The PV is not a destructive vacuole. **(A)** HepG2 cells infected with *Plasmodium berghei* sporozoites expressing the GFP fluorescent protein were labeled with LysoTracker for 10 minutes. They were then monitored by live microscopy at different developmental stages. At the sporozoite stage, there was marked accumulation of LysoTracker-positive vesicles around the parasite, which met the criteria for strong association (the presence of >10 LysoTracker-positive vesicles around the parasites was deemed to indicate a strong association. A weak association was <10 vesicles). The parasites with strong and weak associations were counted and expressed as percentages. Standard deviations are depicted. DNA was stained with Hoechst 33342. Sporozoite (spz) $p = 0.0148$. Early schizont (e-schz) $p = 0.0015$. Late schizont (l-schz) $p = 0.0011$. **(B)** HepG2 cells infected with mCherry-expressing *P. berghei* parasites were fixed at different time points and stained with an antibody specific for LAMP1. DNA was stained with DAPI. Scale bars: 10 μm. Stained cells were then monitored by live microscopy at different stages of parasite development. At the sporozoite stage, marked accumulation of LAMP1-positive vesicles around the parasite was observed. It was deemed to be a strong association if more than 30% of the parasite was covered by anti-LAMP1 antibody. The parasites with strong and weak associations were counted and expressed as percentages. Each bar indicates the average of 3 independent experiments. Standard deviations are depicted. $p < 0.001$ (spz), $p < 0.001$ (e-schz), $p < 0.001$ (l-schz).

Figure 5. Autophagic markers label arrested parasites. **(A)** HepG2 cells infected with fully virulent *Plasmodium berghei*-GFP sporozoites were labeled with LysoTracker-red for 10 minutes. At 48 hours post-infection, the cells were monitored by live microscopy. LysoTracker-positive vesicles around the parasites were counted and scored as strong or weak associations as described in **Fig. 4**. The strongly and

weakly associated parasites were then counted and expressed as percentages. Each bar indicates the average of 3 independent experiments. Standard deviations are depicted. DNA was stained with Hoechst 33342. Scale bars: 10 μm. Arrested p = 0.0298. Developed p = 0.0011. **(B)** HepG2 cells infected with mCherry-*P. berghei* sporozoites were fixed 48 hours post-infection and stained with an antibody specific for LAMP1. DNA was stained with DAPI. Scale bars: 10 μm. The association of LAMP1-positive vesicles with the parasites was scored as strong or weak as before (**Fig. 4B**). The strongly and weakly associated parasites were then counted and expressed as percentages. Each bar indicates the average of 3 independent experiments. Standard deviations are depicted. p = 0.0023 (arrested), p = 0.002 (developed).

Figure 6. Ubiquitination and SQSTM1 labeling during early parasite development. **(A)** GFP-ubiquitin (green)-transfected HepG2 cells were infected with mCherry-*P. berghei* sporozoites (red) and monitored by live microscopy at different developmental stages. Each image depicts the main phenotype quantified at the indicated developmental stage. Scale bars: 10 μm. Quantification was performed visually by counting the parasites that associated strongly or weakly with ubiquitin. If more than 30% of the parasite's periphery was covered with ubiquitin-positive signals, the parasite was considered to be strongly associated. If less than 30% of the parasite's periphery was covered, the parasite was considered to be weakly associated. Each bar indicates the average of 3 independent experiments. Standard deviations are depicted. Sporozoite (spz) p = 0.002. Early schizont (e-schz) p = 0.0037. Late schizont (l-schz) $p < 0.001$. **(B)** HepG2 cells infected with mCherry-expressing *P. berghei* sporozoites were fixed at different developmental stages and stained with an antibody specific for SQSTM1 (green). DNA was stained with DAPI.

Scale bars: 10 µm. Quantification of SQSTM1 signals was performed as described above for ubiquitin signals. Each bar indicates the average of 3 independent experiments. Standard deviations are depicted. Spz $p < 0.001$. E-schz $p = 0.0021$. L-schz $p = 0.042$. **(C)** *Atg*5 WT and *Atg5*-/- cells transfected with GFP-Ubiquitin plasmid were infected with mCherry-expressing *Plasmodium* sporozoites. Live microscopy was performed at 6 hours post infection. Scale bars correspond to 10 µm.

Figure 7. Colocalization of ubiquitin, SQSTM1 and LC3 in infected cells during parasite development. (A) GFP-Ubiquitin and RFP-LC3 double-transfected HepG2 cells were infected with wild type *Plasmodium berghei* sporozoites and monitored by live microscopy at different developmental stages. The sporozoites are labeled by complete colocalization of ubiquitin and LC3, which is lost at later time points. DNA was stained with Hoechst 33342. **(B)** GFP-LC3 (green)-expressing HepG2 cells were infected, fixed at different developmental stages, and stained with an antibody specific for SQSTM1 (red). DNA was stained with DAPI (blue). Scale bars: 10 µm.

Figure 8. Persistence of ubiquitination and SQSTM1 in arrested parasites. (A) GFP-Ubiquitin-transfected HepG2 cells infected with mCherry-expressing *P. berghei* sporozoites were monitored by live microscopy 48 hours post-infection. Scale bars: 10 µm. The strength of ubiquitin-positive staining around the parasite was scored as described for ubiquitin in the legend to Figure **7A**. Each bar indicates the average of 2 independent experiments. Standard deviations are depicted. $p < 0.0001$. **(B)** HepG2 cells were infected with mCherry-expressing *P. berghei* sporozoites, fixed 48 hours post-infection, and stained with antibodies specific for SQSTM1. DNA was stained with DAPI. Scale bars: 10 µm. The strength of SQSTM1-positive staining around the parasite was scored as strong or weak as described for ubiquitin in the

legend of Figure **7A**. Each bar indicates the average of 2 independent experiments. Standard deviations are depicted. Arrested p = 0.0177. Developed p = 0.042.

Figure 9. Assessment of the effect of starvation on parasite liver-stage development by *in vivo* bioluminescence. Balb/c mice were infected by intravenous (i.v.) injection of $1x10^5$ PbmCherry$_{hsp70}$+Luc$_{eef1a}$ sporozoites. Mice were divided into 3 groups: a control group feeding *ad libidum*, a group of mice fasting 12h prior to infection, and 18h post-infection, and a group of mice fasting for 30h following infection. **(A)** parasite development was assessed by whole body luminescence at the indicated time-points (hours post-infection; hpi) in mice. Representative images of one mouse per group are shown. **(B)** ROI measurements for the liver area of all mice (n=9) were recorded as photons per second per area (photons/s/cm^2) for firefly luciferase. **(C)** Balb/c and C57B/6 mice were infected with $2x10^5$ sporozoites, and divided into a control group, or groups fasted for 24 or 36h. For all mice, livers were removed at 40hpi for histology analyses. Sections were stained with H&E, and parasite numbers and sizes quantified. Parasite sizes (**C**) and numbers (**D**) are expressed as percentage to the control. Mean number and parasite sizes of control mice were set as 100%. Experiments were repeated 3-5 times (error bars show SD; * p=0.05; **p=0.01; ***p<0.001).

Figure 10. Assessment of the effect of autophagy induction and inhibition on parasite liver-stage development by *in vivo* bioluminescence. Balb/c mice were infected by intravenous (i.v.) injection of $1x10^5$ PbmCherry$_{hsp70}$+Luc$_{eef1a}$ sporozoites. Mice were divided into: a control group untreated; a control group injected with solution media only; a group treated with rapamycin 12 and 24hpi; a group pre-

treated with rapamycin 12h prior to infection, and 12hpi; a group treated with chloroquine 12 and 24hpi; a group pre-treated with chloroquine 12h prior to infection and 12hpi **(A)** parasite development was assessed by whole body luminescence at the indicated time-points (hours post-infection; hpi) in mice. Representative images of one mouse per group are shown. **(B)** ROI measurements for the liver area of all mice (n=15) were recorded as photons per second per area (photons/s/cm^2) for firefly luciferase. Balb/c and C57B/6 mice were infected with $5x10^4$, $1x10^5$, and $2x10^5$ sporozoites. Histology sections were obtained from infected mice under 3 conditions, namely untreated controls, rapamycin-treated mice, and chloroquine-treated mice. Livers of all mice were removed 40hpi, paraffin-fixed, H&E-stained and analyzed. Parasite sizes **(C)** and numbers **(D)** were quantified for the 3 groups. Average number and parasite sizes of control mice were set as 100%. Parasite numbers and sizes of rapamycin- and chloroquine-treated mice are expressed as percentage of controls. Experiments were repeated in triplicate (error bars show SD;
* p=0.05; ** p=0.01; ***p<0.001; for (B) for simplification * denotes p-value is significant; details of significance are shown in figure S9).

Figure 11. Parasite development after host cell autophagy is blocked. (A) Wild-type (WT) and *Atg*5-/- murine embryonic fibroblasts (MEFs) were incubated in starvation media (EBSS) for 2 hours or maintained in normal media (left panels) before they were fixed and stained then and cells were stained with a monoclonal anti-LC3 antibody, and analyzed by IFA. In subsequent experiments, WT and *Atg5-/-* MEFs were infected with mCherry-expressing *Plasmodium berghei* (right panels). The infected cells were fixed 2 hours post-infection. Then, cells were stained with a monoclonal anti-LC3 antibody, and analyzed by IFA. Scale bars: 10 μm. **(B)** WT and *Atg*5-/- MEFs were infected with GFP-expressing *P. berghei* and fixed 48 hours post-

infection. The total parasites were counted and depicted in the figure. Each bar represents the average of three independent experiments. The standard deviation is indicated. p = 0.0091. **(C)** WT and *Atg*5-/- MEFs were infected with *P. berghei* parasites. In the *Atg*5-/- cells, the medium was either supplemented with additional amino acids (*Atg*5-/- +aa) or left untreated (*Atg*5-/-). Parasites sizes were measured 48 hours post-infection. ***p <0.0001. ns, not significant.

Supplementary figures

Figure S1. LC3 must be correctly processed and lipidated before it can accumulate around the parasite. (A) HepG2 cells were transfected with either GFP-LC3 or **(B)** the GFP-LC3^{G120A} mutant, which does not undergo LC3 processing and lipidation. The transfected cells were then infected with *Plasmodium berghei* parasites expressing mCherry protein and analyzed at different developmental stages by live microscopy. DNA was stained with Hoechst 33342. Scale bars: 10 μm.

Figure S2. The parasitophorous vacuole has a non-degradative character. (**A)** HepG2 cells were transfected with cathepsin D-RFP (CathD-RFP) and infected with *Plasmodium berghei* sporozoites expressing GFP. The infected cells were monitored by live microscopy at different developmental stages. DNA was stained with Hoechst 33342. Accumulation of 10 or more cathepsin D-positive vesicles in the immediate proximity was considered to indicate a strong association. Fewer than 10 vesicles was considered to indicate a weak association. Each bar indicates the average of 3 independent experiments (n = 50 cells per experiment). p = 0.0067 (spz), p = 0.0074 (e-schz), p = 0.00194 (l-schz). DNA was stained with Hoechst 33342. **(B)** HepG2

cells incubated with DQ-BSA red overnight were infected with GFP-expressing *P. berghei* parasites and analyzed at different stages of parasite development by live microscopy. DNA was stained with Hoechst 33342. Scale bars: 10 µm. Quantification and statistical evaluation was performed as described in **A**. Each bar indicates the average of 3 independent experiments (n = 50 cells per experiment). p = 0.0463 (spz), p = 0.0334 (e-schz), p = 0.0015 (l-schz).

Figure S3. Lysosome association with the parasitophorous vacuole (PVM). HepG2 cells were infected with *Plasmodium berghei* parasites and fixed at different developmental stages. The slides were stained with a combination of antisera specific for a PVM marker protein (sporozoite: UIS4; early and late schizont: Exp1) and the lysosome marker LAMP1. Staining of the DNA with DAPI was also performed. LAMP1 colocalizes with the PVM at the early stages of parasite development, which indicates the presence of lysosomes at the PVM at these stages. Scale bars: 10 µm.

Figure S4. Accumulation of LC3 and degradation markers in early-stage parasites. GFP-LC3 transfected HepG2 cells were infected with wild type *Plasmodium berghei* sporozoites, labeled with different lysosomal markers, and analyzed by live microscopy. **(A)** LysoTracker was added to the medium of the infected wells 10 minutes before the analysis at different developmental stages. **(B)** Proteolytic activity was qualitatively indicated by staining with DQ-BSA red. The infected cells were monitored at different developmental stages of the parasite and representative images are presented. **(C)** HepG2 cells were double-transfected with the LC3 and Cathepsin D expression plasmids. Cathepsin D (red) and GFP-LC3

(green) expression is presented for different developmental stages of the parasite. In all experiments, DNA was stained with Hoechst 33342. Scale bars: 10 µm.

Figure S5. Lysosome colocalization with LC3 at early developmental stages. GFP-LC3-expressing HepG2 cells were infected with *Plasmodium berghei* wild-type parasites and fixed at different developmental stages. The slides were stained with antibodies specific for the lysosome marker LAMP1 and with the DNA dye DAPI. LAMP1 colocalizes with the autophagy marker LC3 at the sporozoite stage and during early schizogony. Scale bars: 10 µm.

Figure S6. Galectins are not involved in LC3 recruitment to the PVM. HepG2 cells expressing the indicated YFP-tagged galectins were infected with mCherry *Plasmodium berghei*. Cells were fixed at different time points after infection: **(A)** 6 hpi; **(B)** 24 hpi; **(C)** 48 hpi, and galectins were stained with an antibody against GFP that also recognizes YFP. Cells were stained in addition with Dapi and this was included in the merged images.

Figure S7. Generation and analysis of the *P. berghei* ANKA reporter line mCherry$_{hsp70}$+Luc$_{eef1\alpha}$, expressing mCherry under the control of *hsp70* promoter and luciferase under the control of the *eef1α* promoter.

(**A**) Schematic representation showing the introduction of mCherry-reporter cassette (pL1720) into the GIMO$_{ANKA}$ (line 1596cl1). Construct pL1720 contains the *5'hsp70* (promoter)-mCherry-*3'hsp70* (terminator) cassette and the *5'eef1α* (promoter)-luciferase-*3'pbdhfr/ts* cassette. The construct integrates into the modified *P. berghei 230p* locus containing the *hdhfr::yfcu* selectable marker cassette by double cross-over homologous recombination at the target regions (grey boxes). Negative

selection with 5-FC selects for the transgenic parasite line PbmCherry$_{hsp70}$+Luc$_{eef1\alpha}$ (1868cl1) that have the mCherry/Luciferases cassettes introduced into the *230p* locus and the *hdhfr::yfcu* marker removed. (**B**) Southern analysis of separated chromosomes confirms the correct integration of construct pL1720 into the *P. berghei* genome thereby creating mCherry$_{hsp70}$+Luc$_{eef1\alpha}$. For Southern analysis, PFG-separated chromosomes of the GIMO (ANKA) Motherline[46] as well as clone 1 (cl1) and 2 (cl2) of mCherry$_{hsp70}$+Luc$_{eef1\alpha}$ were hybridized (left hand side) using a mixture of two probes: a control probe recognizing p25 on chromosome 5 (chr. 5) and an h*dhfr* probe recognizing h*dhfr::yfcu*. In addition (right hand side) a 3′ UTR *pbdhfr/ts* probe that recognizes the *hdhfr::yfcu* selectable marker cassette in the GIMO$_{ANKA}$ line in the *230p* locus on chromosome 3 and the endogenous locus of *dhfr/ts* on chromosome 7 of both the GIMO$_{ANKA}$ and mCherry$_{hsp70}$+Luc$_{eef1\alpha}$ cloned lines. In addition, chromosomes are hybridized to a probe recognizing h*dhfr* showing the removal of the h*dhfr::*y*fcu* SM cassette in mCherry$_{hsp70}$+Luc$_{eef1\alpha}$. **(C)** mCherry expression in various liver stages of mCherry$_{hsp70}$+Luc$_{eef1\alpha}$. HepG2 cells were infected with mCherry$_{hsp70}$+Luc$_{eef1\alpha}$ sporozoites and were monitored 12, 48 and 56 hours after infection. **(D)** Luciferase expression in livers of mice infected with mCherry$_{hsp70}$+Luc$_{eef1\alpha}$ 12, 44, 140 hours after intravenous injection of mCherry$_{hsp70}$+Luc$_{eef1\alpha}$ sporozoites. **(E**) mCherry$_{hsp70}$+Luc$_{eef1\alpha}$ parasites have a blood stage asexual multiplication rate and gametocyte production that is comparable to wild type *P. berghei* ANKA parasites.

Figure S8. Fasting and rapamycin treatment induce canonical autophagy in hepatocytes *in vivo*. (**A**) Representative images obtained by intravital microscopy performed in 3 groups of naïve LC3-GFP transgenic mice, namely a) control mice untreated, fed *ad libidum*; b) mice fasting for 30h; and c) 24h post-treatment of mice

with Rapamycin. (**B**) LC3 punctae, representative of autophagy activation, were quantified for all conditions *in vivo* per hepatocyte.

Figure S9. Assessment of the effect of autophagy induction and inhibition on parasite liver-stage development by *in vivo* bioluminescence (details of Fig 10B with individual significance assessments). Balb/c mice were infected by intravenous (i.v.) injection of $1x10^5$ PbmCherry$_{hsp70}$+Luc$_{eef1\alpha}$ sporozoites. Mice were divided into: a control group untreated; a control group injected with solution media only; a group treated with rapamycin 12 and 24hpi; a group pre-treated with rapamycin 12h prior to infection, and 12hpi; a group treated with chloroquine 12 and 24hpi; a group pre-treated with chloroquine 12h prior to infection and 12hpi parasite development was assessed by whole body luminescence at (**A**) 12 hpi, (**B**) 24 hpi, (**C**) 36 hpi and (**D**) 44 hpi in mice. ROI measurements for the liver area of all mice (n=15) were recorded as photons per second per area (photons/s/cm^2) for firefly luciferase. Experiments were repeated in triplicate (error bars show SD;
* p=0.05; ** p=0.01; ***p<0.001

Legends to Videos

Video S1. Intravital observation of a dying late liver-stage parasite removed by autophagy. GFP-LC3-expressing mice were infected with mCherry-expressing *Plasmodium berghei* sporozoites. Intravital imaging of late liver-stage development from 40 hours post-infection until 44 hours post-infection was performed.

Video S2. *In vitro* live imaging of a dying late liver-stage parasite removed by autophagy. GFP-LC3-expressing HepG2 cells were infected with mCherry

expressing *Plasmodium berghei* sporozoites and monitored by confocal live imaging at late schizogony. Images were acquired every 6.5 minutes. Scale bar: 10 μm.

Video S3. LC3 accumulates around invading sporozoites. GFP-LC3-expressing HepG2 cells were infected with mCherry-expressing *Plasmodium berghei* sporozoites and then immediately monitored by confocal live imaging. Scale bar: 10 μm. Images were acquired every 2.06 minutes.

Video S4. Normally developing parasites associate with the loss of LC3 from the PVM. GFP-LC3-transfected HepG2 cells were infected with mCherry-expressing *Plasmodium berghei* sporozoites and monitored by confocal live imaging from early schizogony to late schizogony, starting 24 hours post-infection and continuing until 44 hours post-infection. Images were acquired every 7.7 minutes. Scale bar: 10 μm.

Video S5. LC3 dynamics during schizogony. GFP-LC3-expressing HepG2 cells were infected with mCherry-expressing *Plasmodium berghei* sporozoites and monitored by confocal live imaging from early to late schizogony, starting 24 hours post-infection and continuing until 38.4 hours post-infection. Images were acquired every 7.9 minutes. Scale bar: 10 μm.

Video S6. LC3 dynamics during the entire parasite development period. GFP-LC3-transfected cells were infected with mCherry-expressing *Plasmodium berghei* and monitored from the sporozoite stage (6 hours post-infection) until the formation of merozoites (70 hours post-infection). Images were acquired every 1 hour. Scale bar: 25 μm.

Video S7. Growth impairment and elimination of parasites that cannot remove LC3 from the PVM. GFP-LC3-expressing HepG2 cells were infected with mCherry-expressing *Plasmodium berghei* sporozoites and monitored by confocal live imaging, starting at the schizont stage 30 hours post-infection and continuing until 42 hours post-infection. Images were acquired every 6.9 minutes. Scale bars 10 µm.

Video S8. Lysosome fusion with the parasitophorous vacuole (PVM). LAMP1-GFP transfected HepG2 cells infected with *Pb*Exp1-mCherry-expressing *Plasmodium berghei* sporozoites were monitored by confocal live imaging during early schizogony. Scale bars: 10 µm.

Video S9. Association of ubiquitin and LC3 during sporozoite invasion. HepG2 cells double-transfected with RFP-LC3 and GFP-ubiquitin were infected with wild type *Plasmodium berghei* sporozoites and monitored early after infection (1 hour post-infection). Yellow staining corresponds to colocalization of LC3 and ubiquitin. Images were acquired every 1.36 minutes. Scale bar: 10 µm.

Video S10. Canonical autophagy during schizogony of the parasite. GFP-LC3-expressing HepG2 cells were infected with mCherry-expressing *Plasmodium berghei* sporozoites and monitored by confocal live imaging, starting from late schizogony and continuing until merozoite formation. Monitoring began 55 hours post-infection and continued for 12 hours. Images were acquired every 12 minutes. Scale bar: 10 µm.

Prado, Figure 1

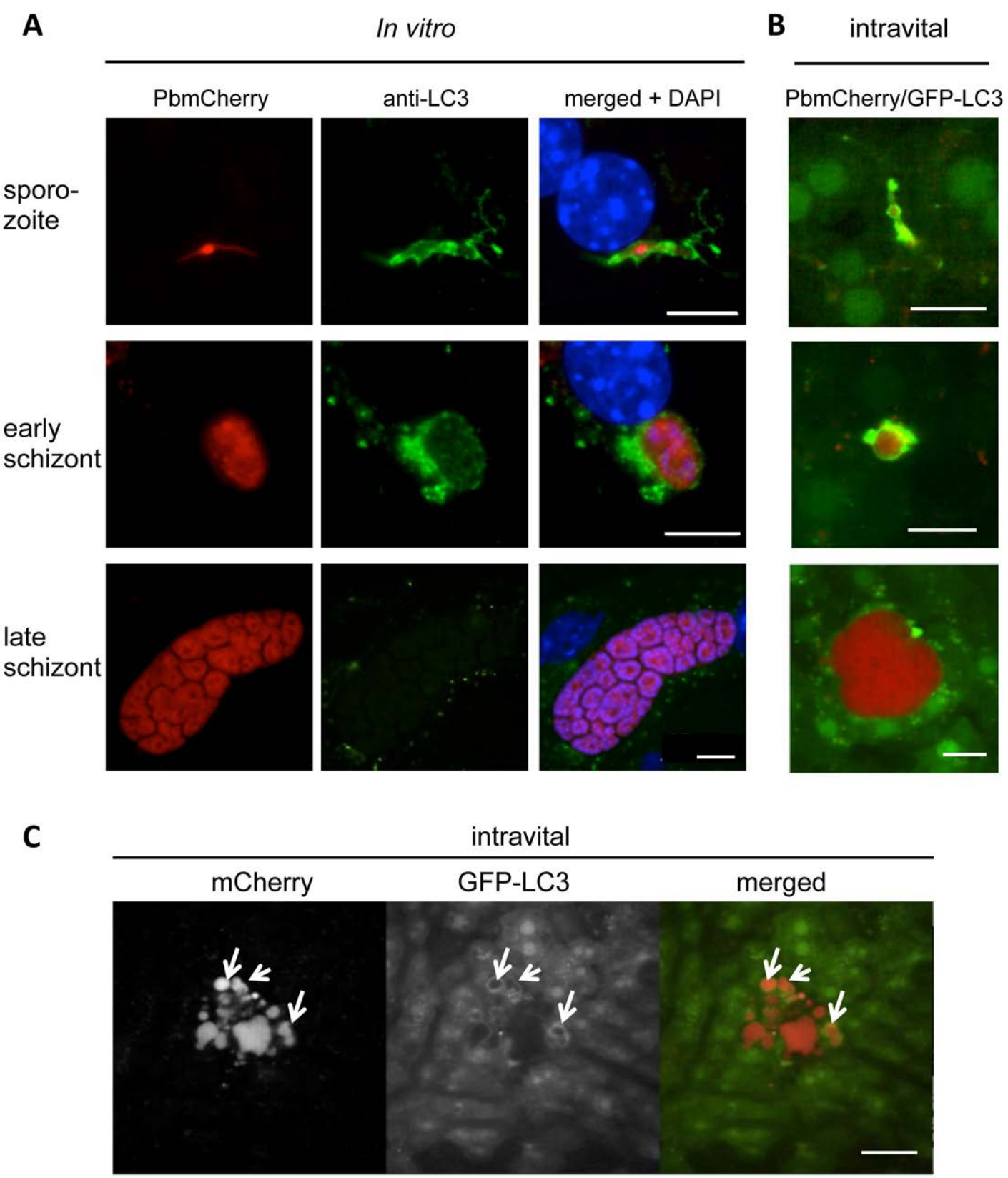

Prado, Figure 2

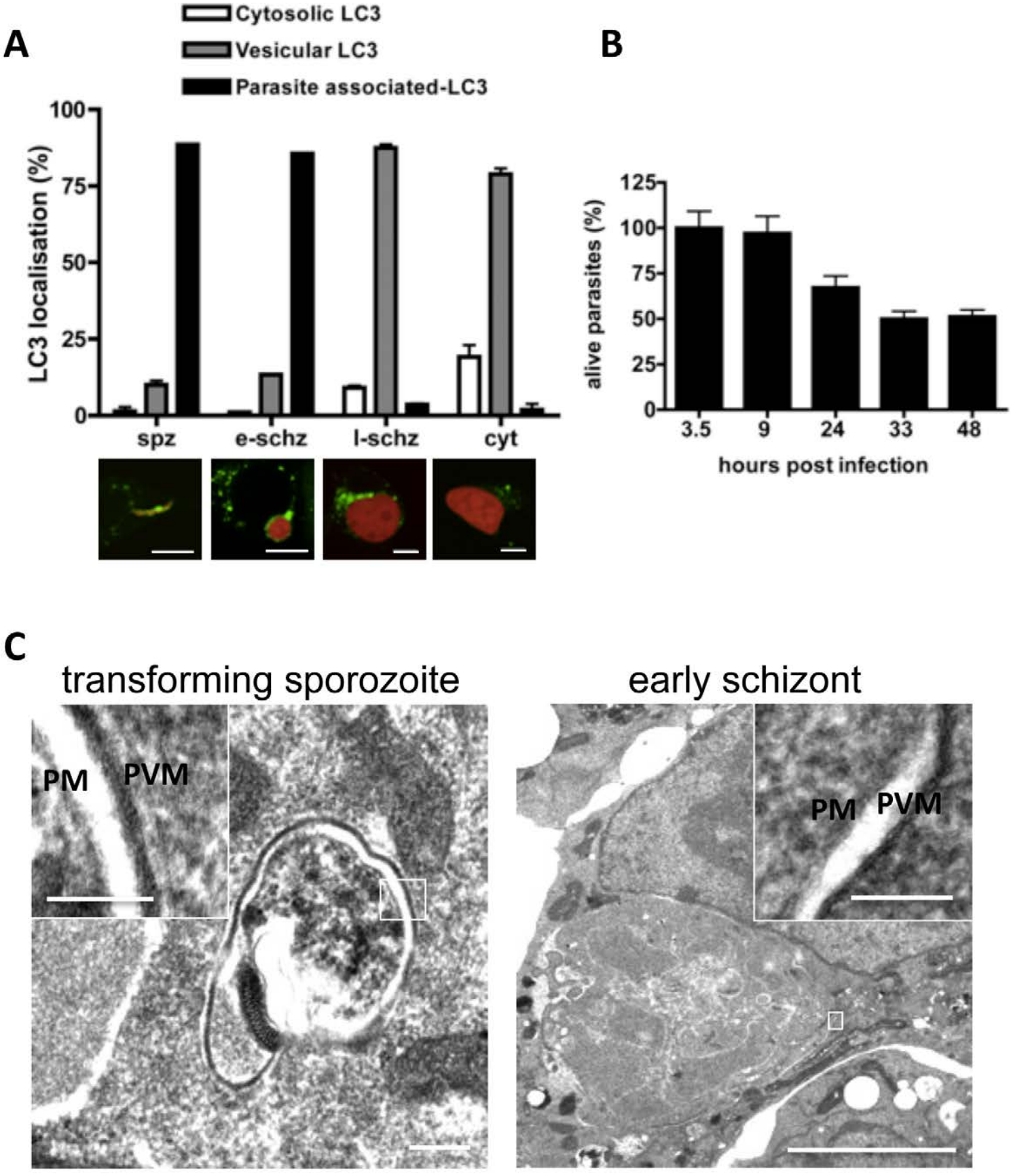

Prado, Figure 3

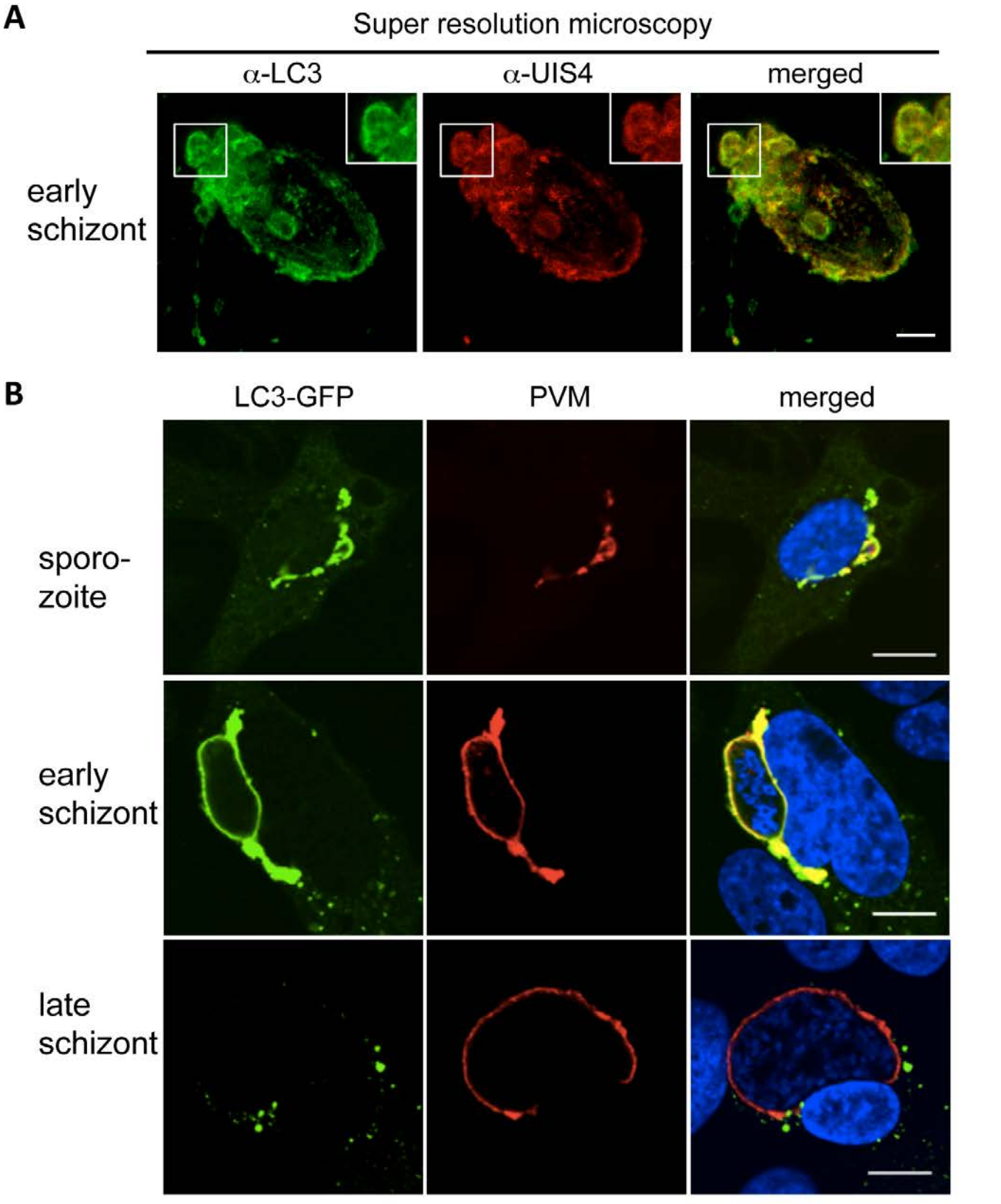

Prado, Figure 4

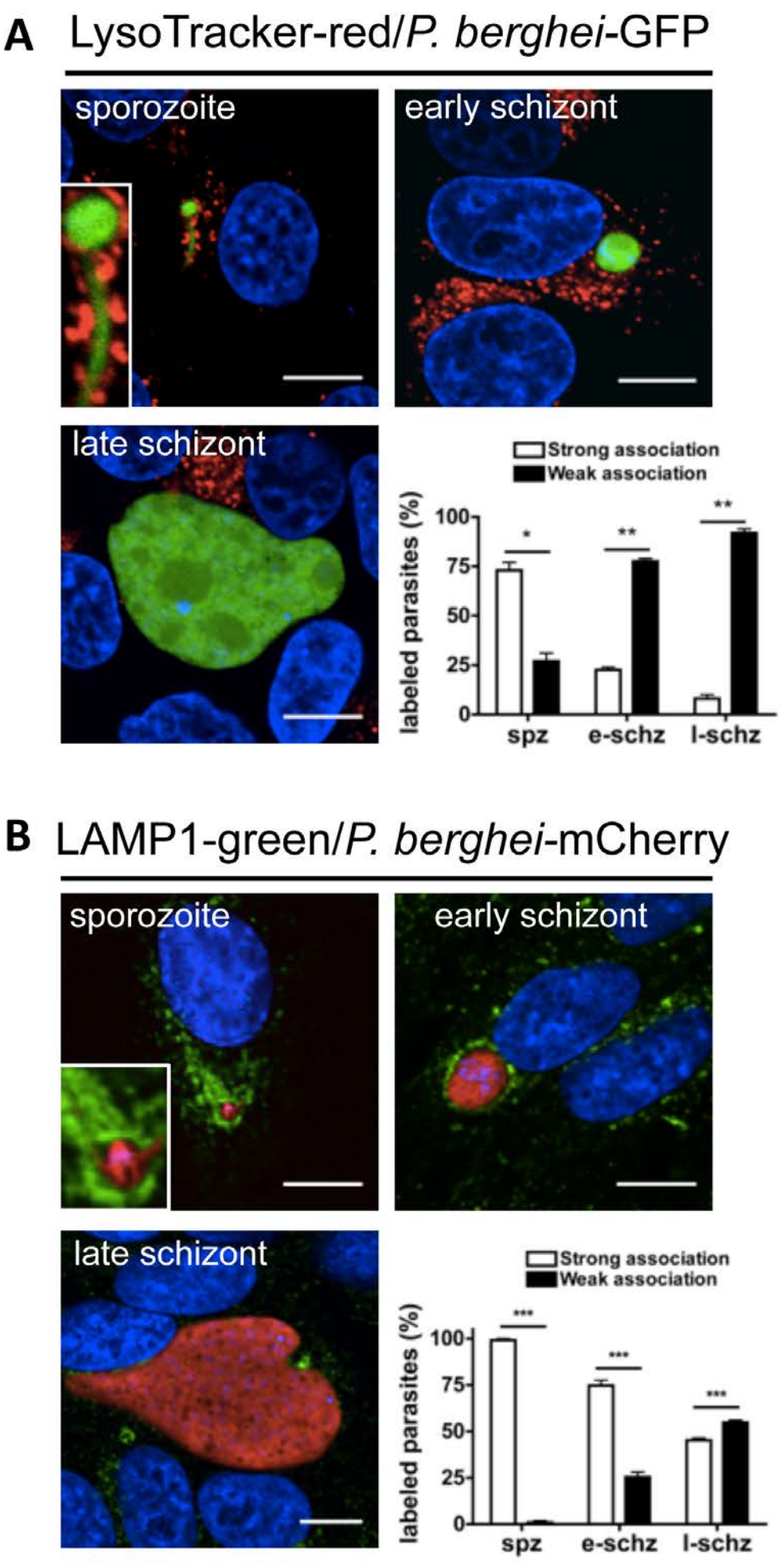

Prado, Figure 5

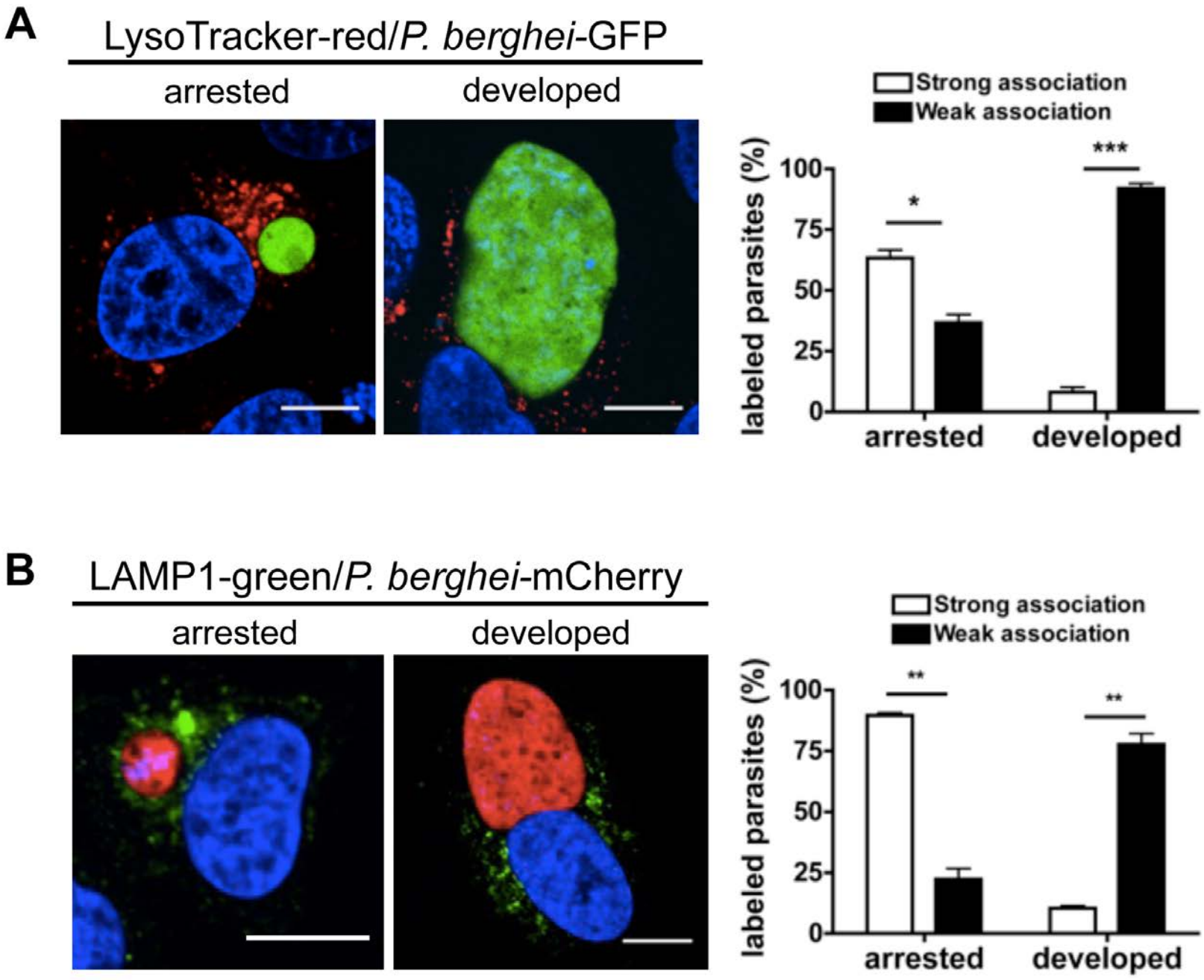

Prado, Figure 6

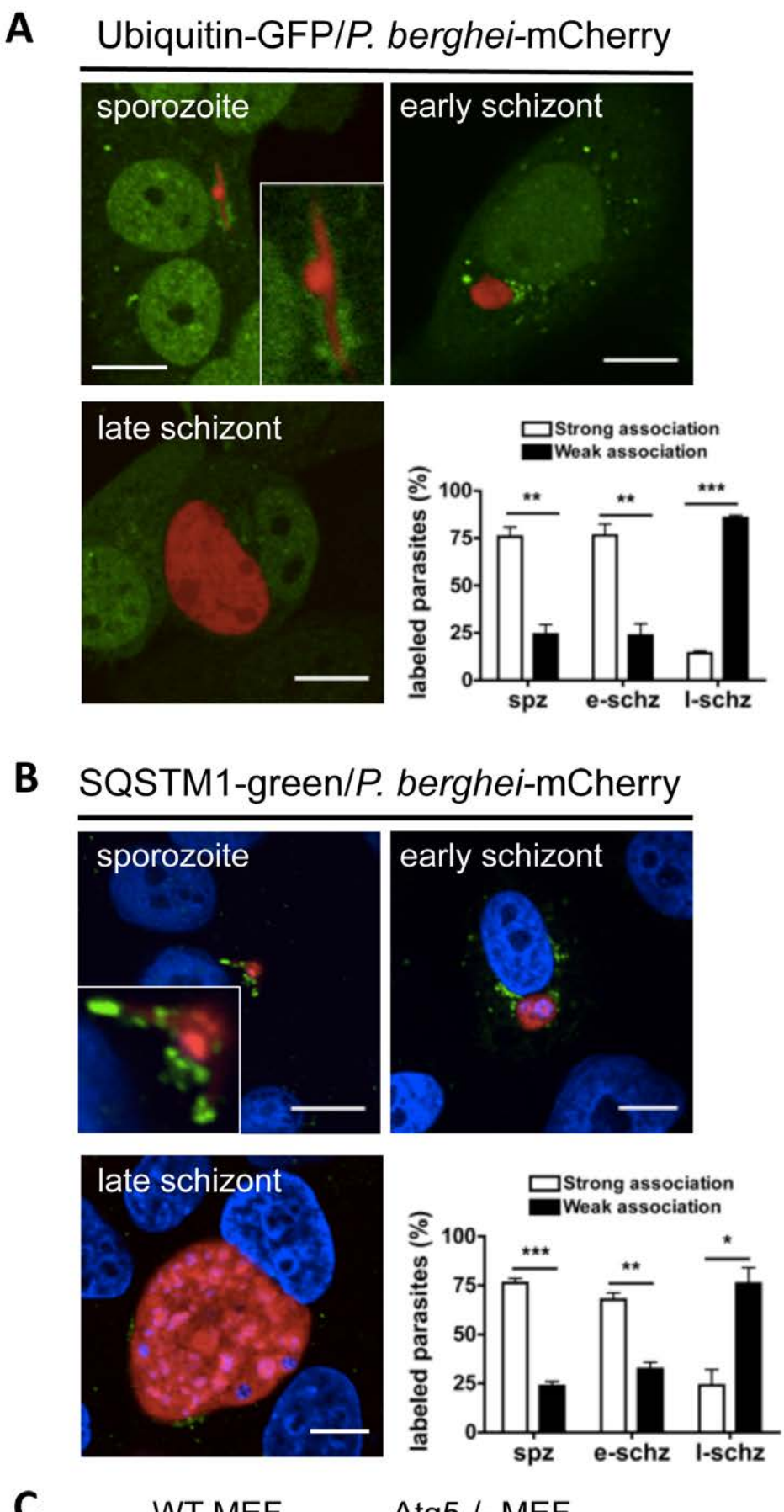

Prado, Figure 7

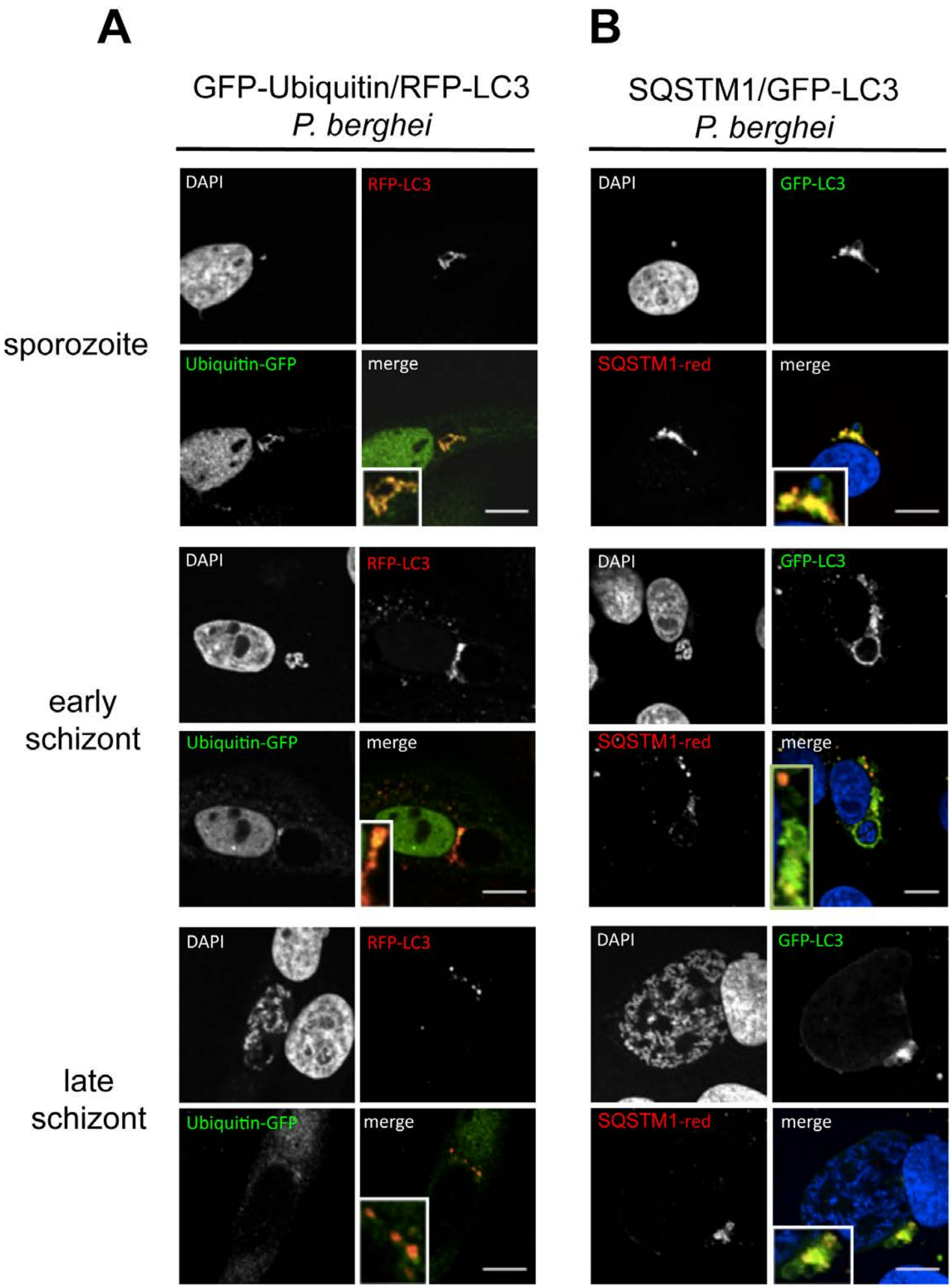

Prado, Figure 8

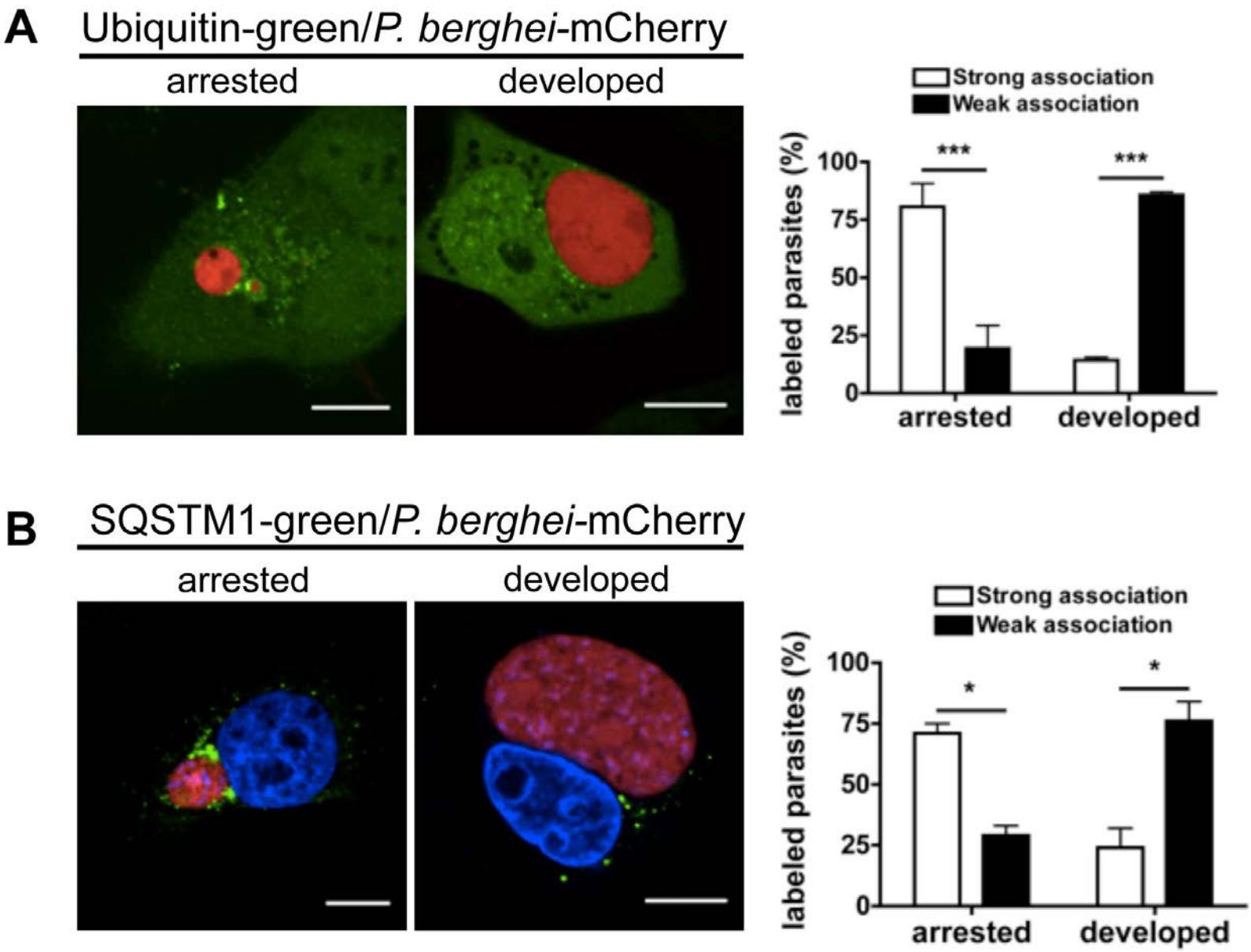

Prado, Figure 9

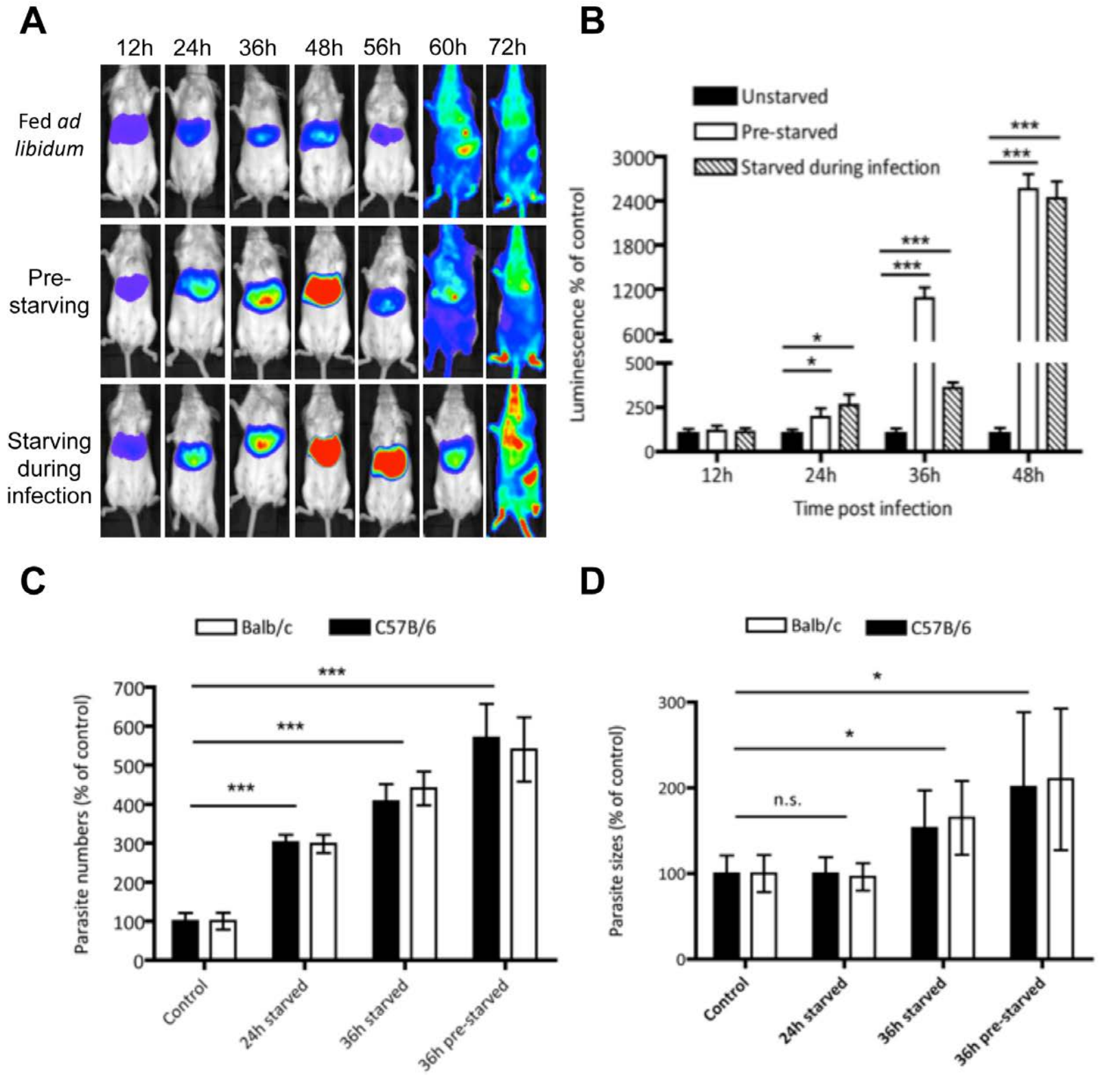

Prado, Figure 10

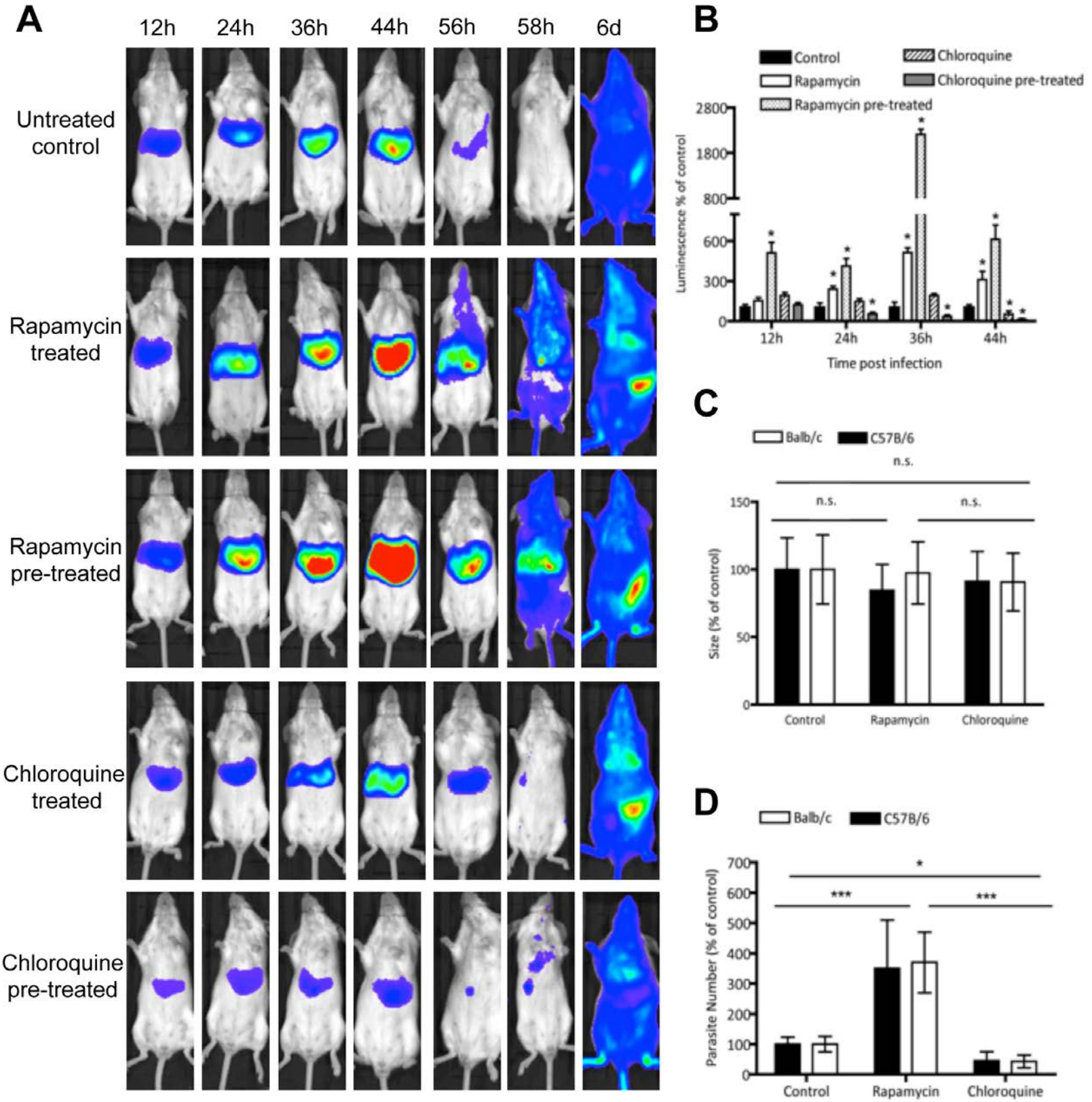

Prado, Figure 11